# Short-term interactions of concrete, biofilm, and seawater in the submerged zone of marine environments for sustainable floating offshore wind turbines

Deeksha Margapuram, Marie Salgues, Raphaël Lami, Benjamin Erable, Michel Groc, Renaud Vuillemin, Bruno Hesse, Laurent Zudaire, Jean-Claude Souche, Florian Stratta, et al.

# Short-term interactions of concrete, biofilm, and seawater in the submerged zone of marine environments for sustainable floating offshore wind turbines

Deeksha Margapuram [a,b,*], Marie Salgues [b], Raphaël Lami [c], Benjamin Erable [d,1], Michel Groc [e], Renaud Vuillemin [e], Bruno Hesse [e], Laurent Zudaire [e], Jean-Claude Souche [b], Florian Stratta [b], Fabrice Deby [a], Manon Thueux [d], Carole Veckerlé [c], Emilie Adouane [c], Alexandra Bertron [a,**,2]

[a] LMDC, Université de Toulouse, UPS, INSA, Toulouse, France
[b] LMGC, IMT Mines Alès, University of Montpellier, CNRS, Alès 30100, France
[c] Sorbonne Université, CNRS, LBBM, Observatoire Océanologique, Banyuls-sur-Mer, France
[d] Laboratoire de Génie Chimique, Université de Toulouse, CNRS, INPT, UPS, Toulouse, France
[e] Sorbonne Université, CNRS, REMIMED FR3724, Observatoire Océanologique de Banyuls, Banyuls-sur-Mer, France

A B S T R A C T

The durability of cover concrete in the submerged zone for floating offshore wind turbines is closely associated to the performance of the cement type used, which also plays a key role in the environmental impact of their construction and operation. A real-world study is conducted by simulating the concrete cover, submerging cementitious materials at a depth of 27 m in Banyuls-sur-Mer, located on the Mediterranean coast of France. The objective was to identify the short-term interactions between cementitious materials, biofilm developing at their surface, and seawater after 30- and 90 days exposure, with emphasis on, (i) the influence of cement type on the microbial composition of biofilm, and (ii) the influence of biofilm and seawater on the microstructural, chemical composition, and mineralogical changes within the cementitious matrix. After 30 days of exposure, scanning electron microscopy coupled to energy dispersive spectroscopy detected the formation of Mg-rich, S-rich, and Cl-rich zones in CEM I and CEM III concrete, while CEM V exhibited the same zonation after 90 days. These findings were corroborated by electron probe microanalysis. After 90 days of exposure, regardless of the cement type, calcium carbonate precipitated at the concrete-biofilm-seawater interface, predominantly in the form of aragonite crystals, as identified by X-ray diffraction analysis. In CEM I concrete, a brucite layer formed immediately beneath this $CaCO_3$ deposit. The bacterial and eukaryotic diversity was identified using 16S rRNA and 18S rRNA sequencing, revealing diverse and dynamic communities over time. The macrofouling species, marine polychaetes (or serpulids), have been identified and considered to be biomineral in origin.

## 1. Introduction

Decarbonizing energy by 2050 will be critical for fulfilling the requirements of the Paris agreement and achieving net-zero $CO_2$ emissions [1]. To attain the latter and comply with green economic growth, clean energy solutions such as offshore wind turbine structures are rapidly expanding across Europe, with a target of 450 GW by 2050 [2]. FOWTs is considered as a suitable solution for water depths ranging from 50 to 200 m [3]. The components of FOWT such as towers and substructures are made of steel, but the use of reinforced concrete (concrete with steel reinforcement) is gradually increasing due to technological advancements and increased size and capacity [4]. The durability of reinforced concrete in submerged zone of marine environments present a considerable challenge to their long-term performance, influencing both the financial and environmental impacts associated with the construction, operation, and maintenance of these infrastructures [5]. Moreover, there are still many questions about the environmental impact of cementitious materials, such as concrete, when deployed at sea, particularly concerning their consequences on marine biodiversity.

Recent studies utilizing Life Cycle Analysis (LCA) models have shown that incorporating supplementary cementitious material blends (55–70 % replacement) in cement production can reduce global warming potential by approximately 50 % (from ~450 to ~240 kg $CO_2$-eq/$m^3$) [6]. Other major benefits of using low-$CO_2$-based binders include

* Corresponding author at: LMDC, Université de Toulouse, UPS, INSA, Toulouse, France.
** Corresponding author.
*E-mail addresses:* margapuram@insa-toulouse.fr (D. Margapuram), bertron@insa-toulouse.fr (A. Bertron).
[1] ORCID: 0000-0002-5332-9622
[2] ORCID: 0000-0002-6144-6810

enhanced concrete durability and promoting biodiversity on concrete surface [7–9]. Understanding marine biodiversity on concrete surfaces is crucial, particularly since interactions between biofilms and concrete in dynamic environments, such as seawater, can notably influence the rate and extent of material deterioration [10]. For instance, the durability of reinforced structures in these conditions is compromised by high chloride concentrations and other aggressive agents like sulfates, magnesium, and carbonates, which can alter the electrochemical properties of steel reinforcement. Ensuring durability in submerged zones depends on the transport property i.e., permeation and its reactivity, which refers to the concrete's ability to interact with seawater ions [8]. Meanwhile, leaching of several minerals from concrete and the ingress of specific ions into the cement matrix can initiate chemical reactions by dissolving portlandite ($Ca(OH)_2$), thereby reducing the pH within concrete.

The major chemical ions in seawater include chlorides, sodium, sulphates, magnesium, calcium, potassium, and carbonates. The contact between concrete surface and seawater thus results in multi-ion attack due to solubility of reaction products resulting in a self-patterning geochemical phenomenon, known as "elemental zonation" [11]. Previous studies [11–13] have documented these findings over exposure periods ranging from 2 to 75 years for portland cements and in some cases, blended cements. These studies highlighted the ingress of seawater ions creating three zones: a magnesium-rich zone, a sulfur-rich zone, and a chlorine-rich zone. However, there is a gap in the literature regarding the deterioration patterns for low-$CO_2$ cementitious materials, such as CEM III and CEM V cement (also known as composite cement) concrete, during short-term exposure in a real submerged zone of marine environments. Furthermore, determining the composition of early marine biodiversity communities, such as bacterial and eukaryotic species on concrete surfaces, is essential as this knowledge provides insights into the biofilm structuring and its potential influence on the alteration of concrete substrate, which is explored in this study.

Biological proliferation or biofouling of concrete surfaces in marine environments are frequently observed and have been reported in the literature on numerous occasions [14–19]. Strictly speaking, biological/microbial proliferation is a natural process that occurs on any solid surface under favorable environmental conditions. Cementitious materials are no exception, even if the initial pH of their surface (between 12 and 13) is not ideal for the growth of most environmental micro-organisms. Biofouling can be divided into microfouling and macrofouling. Microfouling is the initial microbial attachment and macrofouling refers to the settlement of macroorganisms such as (macro and micro-) algae, fungi, larvae, barnacles, polychaetes, and mussels [20]. Biofouling on cementitious materials such as concrete in marine environments is an issue of contention because it is multifaceted [21]. On one hand, micro- and macrofouling can contribute positively by restoring or increasing biodiversity [22], while, on the other, it may lead to biodeterioration or microbially induced deterioration of concrete [23, 24]. For instance, the construction of the FOWTs should aim to mitigate environmental impacts as well as fulfil two key functions: ensuring durability and increasing the ecological value of concrete. This involves attracting marine organisms and thereby preserving marine habitats. Bioprotection, as discussed by Coombes, involves using natural processes or macro-organisms, such as barnacles, to protect concrete structures [25]. However, Coombes contends that bioprotection with barnacles is not the same as the concept of eco-design for structures. Eco-design involves intentional design and construction of structures to enhance ecological value from the start. This approach integrates characteristics that promote biodiversity and creation of habitats for marine life, rather than simply allowing natural colonization. While, studies by *Hughes et al.* [23] have found biodeterioration of concrete due to the growth and development of algal filaments between aggregates and cement interface. Another study by *Jayakumar et al.* [26] demonstrated that algal species, specifically *Chaetomorpha antennina* and its secondary metabolites such as organic acids, have undesirable consequences on concrete surfaces. Early colonists like bacteria, prokaryotes such as cyanobacteria, eukaryotes like microalgae (diatoms), and fungi are abundant planktonic communities that contribute to microfouling on concrete structures in the marine environment [27,28]. Given that biofilms are dynamic, biochemical cues signalled by this layer can have an impact on larval settlement and macrofouling, either directly or indirectly [29]. The description of macrofouling has certainly been the subject of more work. The state-of-the-art suggests that the area covered by biofilm and species such as barnacles (or sessile organisms) may provide benefits in terms of microcrack closure in some places on the exposed surface [19] and a reduction in the rate of chloride migration on areas covered by them [30–32,17]. Another study conducted by *Lv et al.* over a 22-year period confirmed that barnacle settlement area (barnacles acting as barriers) not only increases water absorption resistance of concrete surface, but also enhances the pore structure [33]. There are several gaps in the existing literature, particularly in studies on the submerged zone, biofilm-concrete interactions, and alterations in cementitious matrices based on the binder used, which can then be used to forecast durability performance. This study aims to address these gaps by providing fresh perspectives.

This study aims for a detailed investigation of concrete surface biocolonization dynamics of marine biofilms, microstructural evolution, and chemical composition changes of cement matrix in concrete of three different types of cement, namely, CEM I (Portland cement, considered as reference in this study), and two low-$CO_2$ cements CEM III (OPC-slag blended cement), and CEM V (OPC-slag-fly ash blended cement), after 30- and 90 days of exposure to natural seawater. The assessment of the short-term durability performance of the three binders presented in this study project the early behavior of cementitious materials. These findings provide valuable indications of potential long-term strengths or weaknesses resulting from cementitious material alterations caused by interactions with natural seawater. In this interdisciplinary research study, we first seek to unveil the beginnings of biocolonization/biofouling of concrete surfaces and investigate the composition of the biological community involved in early biofouling as a function of cement type. Then, the microstructural, chemical composition, and mineralogical changes of concrete after exposure to natural seawater was investigated. To investigate these objectives, we submerged plain concrete specimens - simulating concrete cover made from three cement types - at a depth of 27 m in Banyuls-sur-Mer, France.

The first part of the work was concerned with the comprehensive microbiological investigation of early marine biofilms developing on the concrete surface using environmental DNA analysis, field emission gun-scanning electron microscopy (FEG-SEM), and quantitative image analysis of concrete surface. Subsequently, the second part dealt with microstructural development, changes in chemical composition of cement matrix, and mineralogical phases formed in concrete on exposure to seawater for 30- and 90 days. The characterization techniques involved are scanning electron microscopy coupled to energy dispersive

**Table 1**
Chemical compositions of CEM I, slag, and CEM V cements in mass percent.

| Oxide composition (%) | | | | | | | | | |
|---|---|---|---|---|---|---|---|---|---|
| | CaO | $SiO_2$ | $Al_2O_3$ | $Fe_2O_3$ | MgO | $SO_3$ | $Na_2O$ | $K_2O$ | Ignition loss |
| CEM I | 66.1 | 22.9 | 3.0 | 2.4 | 0.9 | 2.3 | 0.1 | 0.2 | 1.3 |
| Slag | 42.1 | 35.1 | 11.1 | 0.4 | 7 | 0.1 | 0.4 | 0.4 | - |
| CEM V | 46 | 31 | 10.1 | 3.4 | 2.6 | 2.6 | 0.24 | 1.20 | 1.8 |

**Table 2**
Mix design of concrete.

| Concrete ID | Aggregates (kg/m$^3$) | Sand (kg/m$^3$) | Cement / binder (kg/m$^3$) | Effective Water (kg/m$^3$) | Water/ Cement |
|---|---|---|---|---|---|
| CEM I | 994.05 | 772.23 | 384.75 | 193.40 | 0.50 |
| CEM III | 994.05 | 772.23 | CEM I – 153.90 Slag –230.85 | 192.38 | 0.50 |
| CEM V | 994.05 | 772.23 | 384.75 | 179.48 | 0.47 |

**Table 3**
Mix design of mortar.

| Mortar ID | Sand (g) | Cement (g) | Water (g) | Water/Binder |
|---|---|---|---|---|
| CEM III | 1350 | CEM I – 180 Slag – 270 | 225 | 0.5 |
| CEM V | 1350 | 450 | 225 | 0.5 |

spectroscopy (SEM-EDS), electron probe microanalysis (EPMA), and X-ray diffractometry (XRD).

## 2. Experimental

### 2.1. Materials

#### 2.1.1. Cementitious materials composition

The two commercial cements, namely, CEM I 52,5 N - SR 5 CE PM-CP2 NF and CEM V/A (S-V) were supplied by *Lafarge* and *Ciments Calcia Heidelberg* respectively. The third cement, CEM III was produced by partially replacing Portland cement (CEM I) with 60 % (by weight) ground granulated blast furnace slag (GGBFS, provided by *Ecocem (France)*). Table 1 shows the chemical composition of the CEM I, slag, and CEM V used in this study.

#### 2.1.2. Preparation of concrete samples

Mix design of concrete specimens with three different cements are summarized in Table 2. The mixes were prepared with a GUEDU type 45 litres NO / PA concrete mixer. We started by adding aggregates to the mixer, followed by cement, and sand in the respective proportions. This dry mixture was mixed for approximately two and half minutes. Following that, we added water and mixed for around two to three minutes. After mixing, the concrete mix was poured in two layers, each vibrating for 15 seconds. They were cast in cylindrical PVC pipe molds (or formwork) of 1.5 mm thickness, 12 cm in diameter, and 6 cm in height. They were poured to a height of 3 cm in plastic molds, with the bottom surface coated with silicon mastic around the perimeter and secured with a weight. The surface cross-section further exposed to seawater was thus in contact with the formwork made of this plastic formwork. The specimens were tightly covered with cling wraps to avoid water evaporation and cured for 36 hours in a curing room at 20℃.

#### 2.1.3. Preparation of mortar samples

Table 3 summarizes two different types of mortar specimens prepared using CEM III and CEM V cements. They were prepared in accordance with the European standard NF EN 196–1 [34], having a water-to-binder ratio of 0.5. The mortar samples were cast in the same PVC molds/formwork as concrete specimens. They were poured to a height of 1.5 cm in molds, covered with silicon around, and secured using a weight. The curing procedure was the same as for concrete specimens.

### 2.2. Description of field experiment

#### 2.2.1. Exposure site / study area

The experiment was carried out using REMIMED platform means (instrumentation, vessels, and diving service) at SOLA station (shown in supplementary material), historical observation points of the Observatoire Océanologique de Banyuls (42°29.357'N / 3°8.645-'E, 27 m water depth, 1 km offshore, Bay of Banyuls-sur-Mer, south-west of the Mediterranean coast of France). This site, which has been monitored for decades by the OOB, is situated in the Parc Naturel Marin du Golfe du Lion and close to the Réserve Naturelle Marine de Cerbère-Banyuls. Station SOLA, at the outlet of the Gulf of Lion influenced by continental inputs and general circulation, is integrated in coastal observation networks (SOMLIT and COAST-HF).

#### 2.2.2. Affixing cementitious samples to glass reinforced plastic (GRP) grating

Concrete and cement mortars in their PVC formwork was set on a grating support intended for exposure to seawater. The grating shown in Fig. 1 constitutes of a moulded glass reinforced plastic with a steel frame. The length and width of the grating is 120 cm. The mesh size opening is 4 cm × 4 cm with a thickness of 4 cm. They were separated into four zones (as shown in Fig. 1) and secured at various corners using self-locking plastic straps. The four ends of the grating are tied to a nylon coiled rope of thickness 4 cm. This rope consists of polyethylene mooring buoy ball to stabilize the grating in deep waters. As shown in Fig. 1, about nine buoys are put together on one side (facing the top),

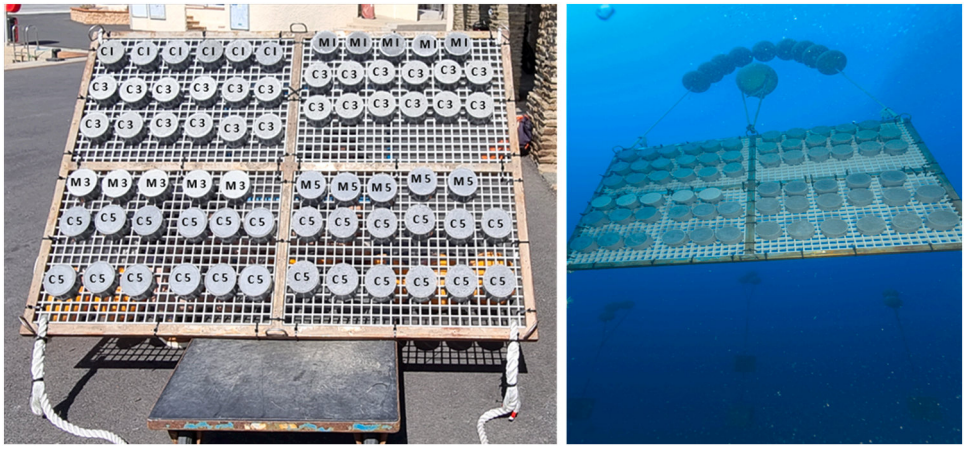

**Fig. 1.** From left: On-site experimental setup before immersing the grating with cementitious specimens into sea water. C and M stand for concrete and mortar with 1,3,5 for CEM I, CEM III, and CEM V cements respectively. The photo on the rightside was captured after one week by scuba diver Bruno Hesse wherein the grating was placed at a depth of 27 m.

while the other end (downside) is tied to a ballast (concrete slab). The grating is oriented southward, with the ocean currents running perpendicular to it.

The grating, housing the cementitious materials were submerged at a depth of 27 m in SOLA station (shown in Supplementary material S1) in the second week of September 2022. The regional technological platform REMIMED (*Réseau Marin Instrumenté en MEDiterranée*) provided all services and support throughout the immersion.

#### 2.2.3. Sampling

The first sampling was conducted in the second week of October, after 30 days of immersion, the second sampling happened in the second week of December, 90 days later, in the same year.

### 2.3. Monitoring and analyses of cementitious specimens and surface colonization

The first section focuses on quantification of area colonized by microorganisms on concrete surfaces using image analysis, advanced molecular techniques such as environmental DNA analysis to characterize microbial communities in biofilms, and microphotographic illustrations of marine biofilms using FEG-SEM. In the second section, the microstructure, chemical composition changes, and mineralogy of concrete specimens are characterized using analytical techniques such as SEM-EDS analysis, EPMA, and XRD.

#### 2.3.1. Surface colonization and biofilm characterization

After 1, 30, 60, and 90 days, photographs were taken, and visual observations were recorded. Further, image analysis was used to quantify concrete surfaces and distinguish the microbially colonized and non-colonized areas at 90 days of exposure. In the case of marine biofilms, biofilms covering mortars surfaces were microphotographed using FEG-SEM. Lastly, biofilms were carefully removed and characterized using Environmental DNA analysis after 30- and 90-day exposure.

*2.3.1.1. Image analysis.* Image analysis software complements visual inspection. We used this software to quantify the area colonized by marine organisms, notably macrofouling species and marine algae, over time for all concrete surfaces.

The raw images were captured underwater at 27 m with Nikon D800 digital camera. The acquired raw image files (NEF format) were first processed digitally using UFRaw software to rebalance colors (as shown in Figure S2 in the supplementary material), simplify image segmentation by isolating the fundamental elements colonizing the concrete surfaces with a simple automatic thresholding operation. The UFRaw development steps included selecting a white balance to mitigate some of the effects of underwater filming (the elimination of red and then green wavelengths). The changes involved altering the colorimetric properties of the images, specifically accounting for the high attenuation in the reds caused by water absorption at these wavelengths. Additional information is available in the supplementary material.

The following procedure was performed using ImageJ 1.38x software to quantify and distinguish the marine fouler organisms such as sessile organisms, algae, and the non-colonized concrete's top surface [35]. The threshold colour in the YUV Lab colour space was utilized to quantify the biofouling species, such as sessile organisms such as serpulids, algae, and the non-colonized concrete areas [36]. By adjusting the values of Y and UV, the area covered by serpulids, and algae was respectively highlighted. The resulting images were processed with a binary system that uses black and white pixels [36], and references therein. The data is further collated and expressed as a percentage of total area fraction covered by serpulids and algae. The mean and standard deviation for the total area colonized, serpulids, and algae were calculated for six images in CEM III and CEM V, as well as two images in CEM I. The biocolonization (area colonized by microorganisms) at 30 days was not quantified as it was challenging to distinguish between colonized and non-colonized concrete surface areas.

*2.3.1.2. Field emission gun-scanning electron microscopy (FEG-SEM).* FEG-SEM is used to observe the surface of cementitious materials at broad magnification levels, including the nanometer scale of microorganisms. This technique qualitatively complements other techniques by providing important information about the appearance, size, and organization of microbial cells in the biofilm [37].

Observations of the biofilms formed on the various mortars were carried out in the "Analysis and Processes" Service of the Chemical Engineering Laboratory on a Leo 435 VP-Carl Zeiss SMT microscope (JEOL JSM-7100F + EDX Oxford ASDD X-Max 50 $mm^2$). SEM observation of biofilms requires pre-treatment of the colonized samples. This treatment consists of three successive steps: fixation, dehydration, and metallization. For the first step, fixation, samples are immersed in a fixation bath containing 2 volumes of 5 % glutaraldehyde, 1 vol of phosphate buffer (0.4 M at pH 7.4) and 1 vol of distilled water for 25 minutes. The samples were then washed thoroughly in two successive baths for 20 min using a solution composed of 1 vol of phosphate buffer (10 mM - pH 7.4), 2 volumes of 0.4 M sucrose and 1 vol of distilled water. The second step is dehydration, which follows step one. This step is essential to prevent volatile water from disturbing the vacuum in the SEM chamber. Dehydration is carried out gradually to avoid osmotic stress for microorganisms adhering to the sample to be analyzed. First, the sample is immersed successively in baths (water/acetone) with increasing proportions of acetone: 50 %, 70 % and 100 % for 5 minutes, then the sample is placed in a solution containing 50 % acetone and 50 % hexamethyldisilazane (HMDS) for 35 min, and finally in a bath of 100 % HDMS until the solvent has evaporated completely. The final step is metallization. Prior to microscopic observation with FEG-SEM, the dehydrated samples were cold sputtered with a thin layer of gold of around 10 nm to make the surface of the sample conductive.

*2.3.1.3. Environmental DNA analysis, bioinformatics, and statistical analysis – advanced molecular approach.* DNA samples were collected and prepared following protocols previously implemented at the lab and published [38,39]. Rosella Biosystem facilities performed the high-throughput sequencing following their routine protocols. Briefly, 16S rRNA, 18S rRNA genes, and ITS genomic fragments were separately amplified by PCR using respective primers 341 F/1391 R [40,41], 391 F/1626 R [42] ITS-u1/ITS-u4 [43]. The ZymoBIOMICS Microbial Community DNA Standard (ZymoResearch, USA) was used as positive control. A 30-cycles PCR was conducted using the UCP Multiplex PCR Kit (Qiagen, USA) under the following conditions: 95°C for 15 min, followed by 30 cycles of 95°C for 30 s, 55°C for 30 s, and 72°C for 3 min, after which a final elongation step at 72 °C for 10 min was performed. After amplification, librairie preparation and indexing were performed with the Native Barcoding 24 kit V14 (Oxford Nanopore Technologies, UK). Sequencing was finally performed on a MinION following the manufacturer's guidelines and using MinION flow cells (R10.4.1) (Oxford Nanopore Technologies, UK). Briefly, bioinformatic analysis relied first on a base calling step which was performed using Dorado v0.3.3 in simplex super accurate mode using model v4.2.0 and default parameters. Then, the obtained fastq files were filtered for read length using Seqkit v2.1.0 [44] keeping discarding reads below 500 bp and above 2000 bp. Subsequently, the deconvolution of the 16SrRNA genes, 18SrRNA genes and ITS amplicons was conducted. Before taxonomic assignment by Kraken2 v2.1.2 [45] based on *Silva* (v138.1) [46] and *Greengenes* (version of 03.06.2017; DeSantis et al., 2006) [47]. Data analyses were then conducted with the R package [48] Phyloseq. DNA sequences were submitted to NCBI (Bioproject PRJNA1088521, Biosamples SAMN40475501 to SAMN40475506).

**Table 4**
Chemical oxide compositions of hydrated cement paste for CEM I, CEM III and CEM V control concrete specimens by EPMA (average value of 100 points).

| CEM I | | | | | | | | | | |
|---|---|---|---|---|---|---|---|---|---|---|
| CaO | $SiO_2$ | $Al_2O_3$ | $Fe_2O_3$ | MgO | $SO_3$ | $Na_2O$ | $K_2O$ | Cl | $TiO_2$ | Other oxides + $H_2O$ |
| 35.64 | 23.12 | 7.79 | 2.62 | 1.87 | 2.9 | 0.28 | 0.76 | 0.035 | 0.43 | 24.46 |
| **CEM III** | | | | | | | | | | |
| 38.82 | 23.77 | 4.55 | 1.83 | 1.55 | 2.93 | 0.33 | 0.19 | 0.17 | 0.23 | 25.63 |
| **CEM V** | | | | | | | | | | |
| 37.02 | 23.36 | 7.17 | 2.52 | 1.42 | 2.79 | 0.37 | 0.77 | 0.04 | 0.35 | 24.19 |

*2.3.2. Chemical and mineralogical analyses of cementitious materials*

All the chemical and mineralogical analyses were conducted on cementitious materials, namely, concrete specimens at 30 and 90 days of exposure, along with control specimens.

*2.3.2.1. SEM - EDS.* Scanning Electron Microscopy coupled to Energy Dispersive X-ray Spectroscopy (SEM-EDS) was used to characterize the microstructure of concrete exposed to sea water. A field emission SEM microscope (JEOL JSM-6380LV with accelerating voltage 15 kV) in backscatter electron (BSE) mode was used to collect images. SEM equipped to EDS detector (Rontec XFLASH 3001) provides element specific mapping of a surface. The various steps involved in the preparation of flat-polished specimens are as follows. After the respective exposure duration (say, 30 and 90 days), concrete specimens were collected from sea water, dried, and used for microstructural investigations. The cylindrical specimen was sawn using a diamond saw perpendicular to their axis to characterize the microstructure of plane top surface (exposed to seawater) of all materials. They were further immersed in an epoxy resin (resin and hardener Presi Ma2+ or Araldite 2020) in 25 mm plastic mold. After 24 hours, they were polished using silicon carbide discs (Presi) of grain size of 26 μm (600), 22 μm (800), 15 μm (1200), and 10 μm (2000) and then coated with a thin layer of carbon [49,50]. Backscattered Electron (BSE) imaging mode was used to obtain information of the top surface of concrete specimens. BSE images were taken at 50x magnification to record the overview of the top surface, and 200x to analyze the chemical (EDS analysis) and morphological changes of the hardened cement paste.

*2.3.2.2. EPMA.* Electron probe microanalysis (EPMA) was performed using CAMECA SX FIVE with an accelerating voltage of 15 kV, a current of 10 nA, and a scanning area of the beam was 2*2 μm. EPMA, being a quantitative technique, was used to determine the chemical composition of different hydrated cement pastes. The analysis was done on flat-polished concrete specimens on the top side exposed to sea water. The sample preparation procedure is the same as for SEM-EDS. Certain specific points were examined excluding the aggregates and anhydrous cement grains. The elements investigated were Ca, Si, Al, Fe, Cl, Mg, S, K, Na and Ti. Before each series of measurements, the equipment was calibrated with known chemical compositions of natural and synthetic standard materials. Quantitative measurements yield the X-ray intensity emitted by a particular element, and this intensity is compared with the standard of the same element. The results obtained are expressed in terms of mass percentages of the respective elemental oxides. In general, the total percentage for cementitious materials is around 75–80 %, with the remaining percentage attributed to the presence of hydrogen, carbon, oxygen, phosphorus, and some trace elements not included in the program analysis. However, the microprobe data were analyzed according to a method published by *Bertron et al.* to assess the absolute oxide composition varying over time [49]. Table 4 shows the average oxide composition of various compounds in CEM I, CEM III, and CEM V control concrete prior to seawater exposure.

*2.3.2.3. XRD.* X-ray diffraction (XRD) was adopted to identify the mineralogical phases of concrete specimens. The measurements were carried out on concrete specimens of three different cement types in function of depth of sound and altered zones after 30 and 90 days of exposure to seawater. The protocol developed by *Bertron et al.* for sample preparation and XRD measurements was followed here [51]. The control concrete specimens were analyzed after 8 weeks of curing. Data was collected with a Brucker D8 diffractometer in $2\theta$ configuration, 4–70°, 0.25 s per step in 0.02° increment, using a monochromator incident beam, and CuKα radiation (λ = 1.54 Å, 40 kV, 40 nA, 15 minutes) with a rotating sample holder.

## 3. Results

### 3.1. Visual observations of concrete surface

In a pioneering effort, we report the results of visual observations of marine microfouling preceding macrofouling (Fig. 2) on the top surface of concrete of three different cement types, namely, CEM I, CEM III, and CEM V, after 1, 30, 60, and 90 days. The photographs clearly indicate that, at 30 days of exposure, algal assemblages have grown and developed on concrete surfaces. Following 60 days exposure, marine invertebrates, particularly juvenile and very few adult sessile organisms (known to be calcareous in chemical composition [59]), appear on concrete surfaces. Finally, after 90 days, we see that CEM III and CEM V cements are substantially colonized by sessile organisms with algal areas. While CEM I maintain nearly the same level of macro-colonization. Overall, micro- and macrofouling evolve dynamically. It is also pertinent to note from the photographs that non-colonized areas are reducing over time. The following findings from image analysis corroborate the assessment of visual appearances, specifically the differentiation between biocolonized and non-colonized areas.

### 3.2. Quantification of microbial colonization of concrete surface using image analysis

Visual inspections indicate the growth of macro fouling species, namely, calcareous serpulid tubes after 60 days (Fig. 2A). Furthermore, after 60 and 75 days (not shown here), the concrete surfaces of all cement types appear strikingly similar. As a result, the presented image analysis results were investigated after 75 and 90 days. Fig. 2B shows the percentage area covered by macro fouling organisms, i.e., serpulid tubes (also known as serpules), algae, and the total area after 75 and 90 days of exposure to seawater. The formation of bacterial biofilm starts within minutes of immersion in seawater [28,52], but the macrofouling, i.e., evolution of macroorganisms such as serpulid tubes is observed between 50 and 60 days (shown in Section 3.1). Based on the total area of biocolonization following 90 days of exposure, we find that CEM I and CEM III cement types have a slightly higher total percentage fraction covered than CEM V cement. From the data, we notice a 15–20 % increase in total colonization between 75 and 90 days. The image analysis data is aligning with visual inspections, which show an enrichment of serpulid species on concrete surfaces, with CEM III covering a slightly wider area than the other two cement types.

According to our findings, image analysis is an effective tool for measuring both the total area of biocolonization and the area covered by serpulid tubes on the concrete surface. The relative area covered by algal

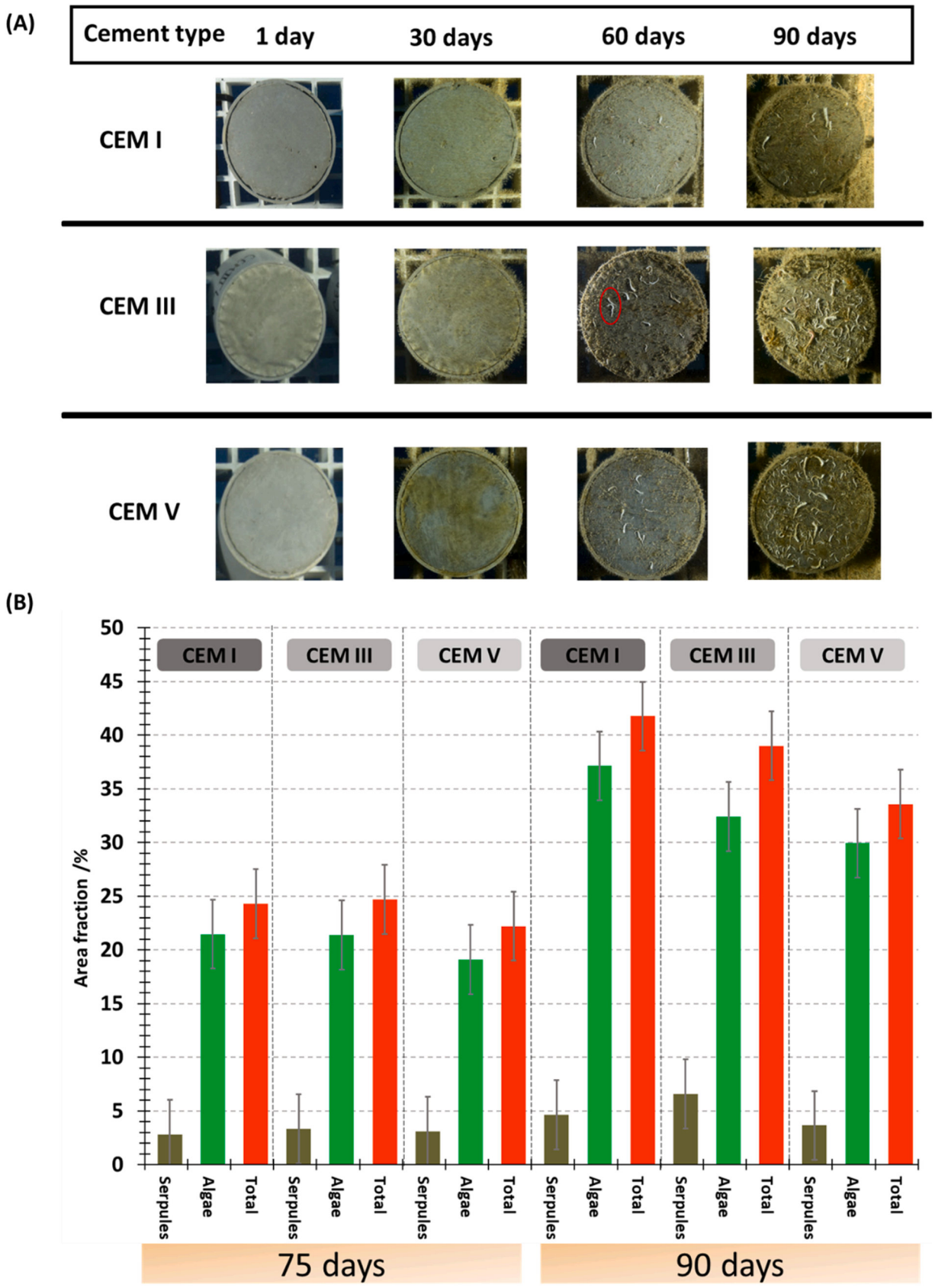


**Fig. 2.** (A) Photographic images (captured by Bruno Hesse) of the top surface of concrete showing evolution of biofilm formation at different immersion times (in days). An example of calcareous sessile organism (serpulid tubes) circled in red on CEM III concrete surface after 60 days of exposure; and (B) Bar graph showing the area colonized (in terms of percentage) by serpulids, algae, and total macrofouling on top surfaces of concrete analyzed using image analysis at two different exposure times.

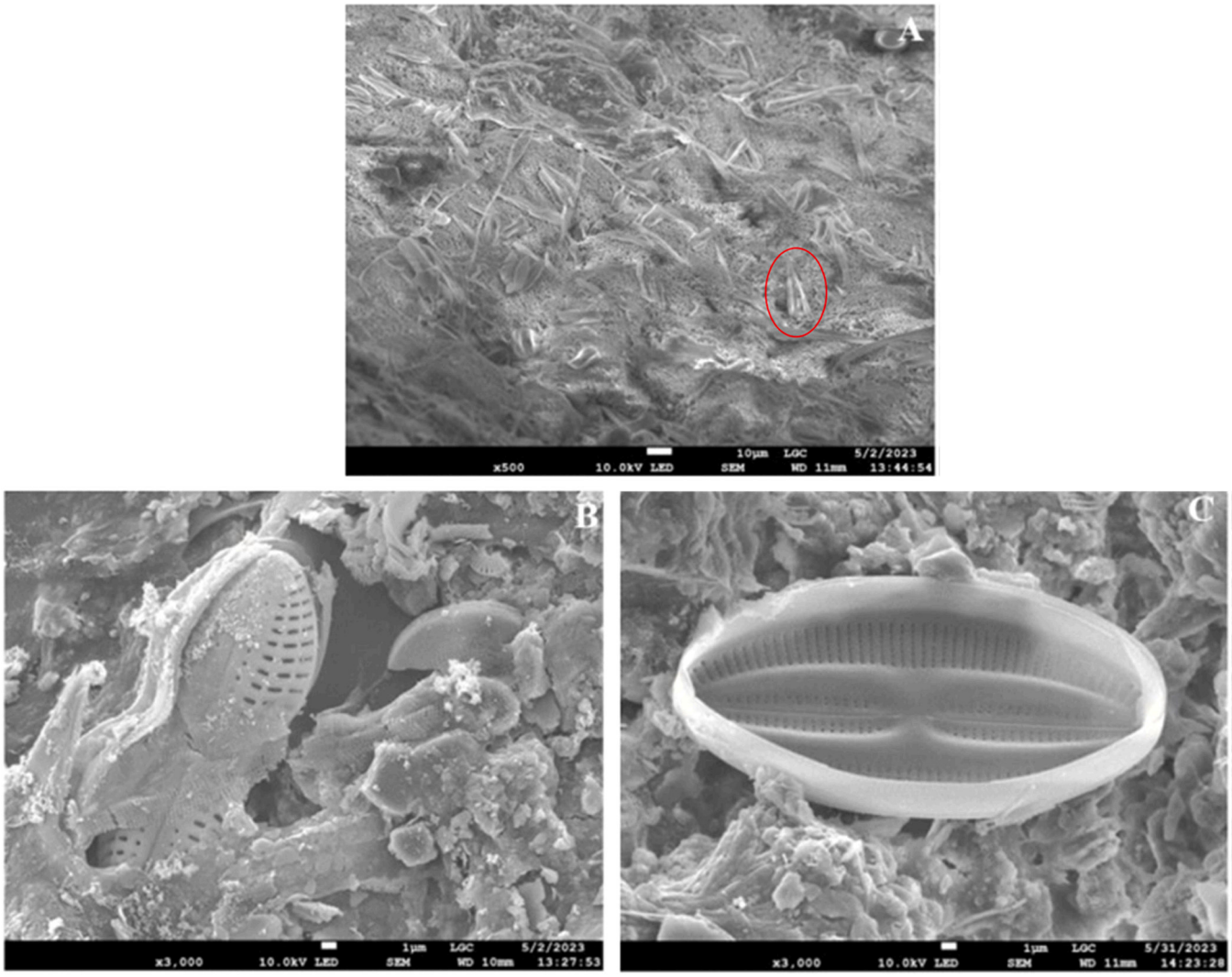


**Fig. 3.** FEG-SEM image of: (A) Biofilm containing diatoms (circled in red) on the surface of CEM V mortar at 30 days of exposure; (B) Diatom on CEM III mortar surface at 30 days exposure; and (C) Magnified view of pennate diatom on the surface of CEM V mortar at 90 days exposure.

groups on the concrete surface should be interpreted with caution, and additional studies, such as confocal microscopy, are required to supplement accurate data on algae distribution.

### 3.3. Microscopic illustration of marine biofilm on cementitious surface

Fig. 3A, B, and C shows FEG-SEM observations of diatom frustules in marine biofilm on mortar surfaces at different exposure times. Fig. 3A shows the abundance of diatoms on the surface of CEM V mortar after 30 days of exposure to seawater. Fig. 3B and C illustrates individual diatom frustules that appear to be embedded in a mineral (mostly calcium carbonate deposit) on the surface of CEM III and CEM V mortars respectively. These findings clearly demonstrate the presence of biocolonization on the surface of the materials by microorganisms other than bacteria, at least by diatoms (eukaryotes).

### 3.4. Investigation of microbial communities based on cement type

Bacterial colonization of surfaces emerged as a crucial factor during both 30 and 90-day samplings, showcasing a diverse array of pioneer colonizers (shown in Fig. 4). Within the biofilm, Proteobacteria demonstrated dominance, particularly Alphaproteobacteria (34.1 % ± 8.6 of total sequences) and Gammaproteobacteria (23.5 ± 9.4). Additionally, Planctomyceta, Firmicutes, and Bacteroida were prevalent, constituting 1–15 % of the biofilm. Interestingly, no significant diversity variations were observed between sampling months or types of cement ($P>0.05$).

Eukaryotic colonization also played a significant role during both samplings, evident through the utilization of the 18S rRNA and ITS genetic markers (shown in Fig. 5 and ITS genetic marker data shown in supplementary material). The 18S rRNA marker highlighted substantial biofilm colonization by Nematozoa (47.1 % ± 14.5 of total sequences in October), Arthropoda (8.1 % ± 3.8), Ascomycota (13.1 % ± 2.9 in December), and fragments of Embryophyta (33.8 % ± 9.8). Meanwhile, the ITS genetic marker unveiled diverse colonization by Oomycota (0–14 %), Cnidaria (38.9 % ± 16.4), and Arthropoda (4.9 % – 65.8 %). The 18S rRNA marker indicated significant differences in eukaryotic colonizing diversity between 30 days and 90 days samplings ($P<0.05$), but not between types of cement ($P>0.05$), a result consistent with the findings from the ITS genetic marker.

Notably, an exception was observed in the CEM III sample collected in December. Here, the colonizing diversity appeared significantly different ($P<0.05$) from all other samples, as indicated by the ITS genetic marker. This sample was dominated by an unidentified group of Arthropods, comprising 65.8 % of total sequences.

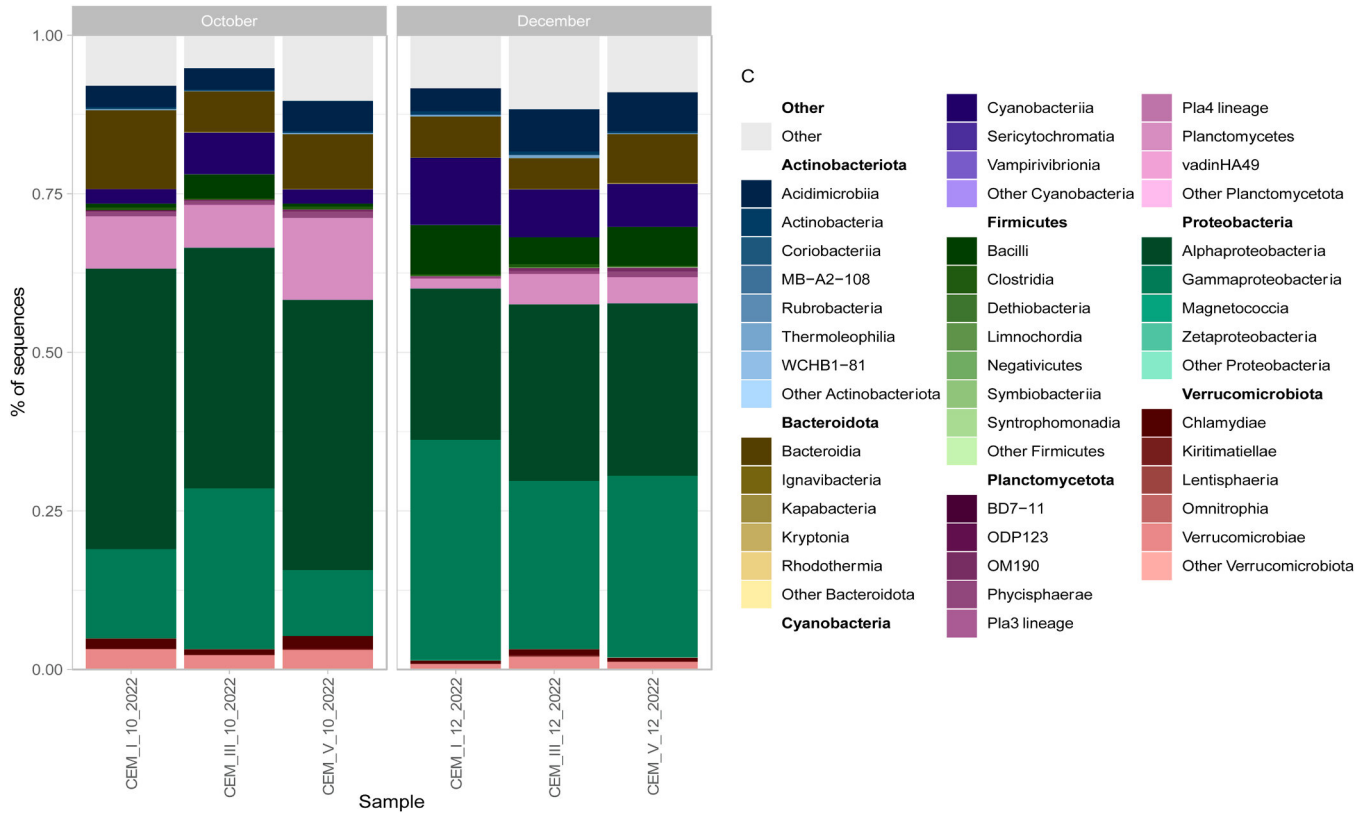


**Fig. 4.** From left to right: Bacterial diversity (16S rRNA) of marine biofilms colonizing the three different types of cement immersed for 30 (October) and 90 (December) days.

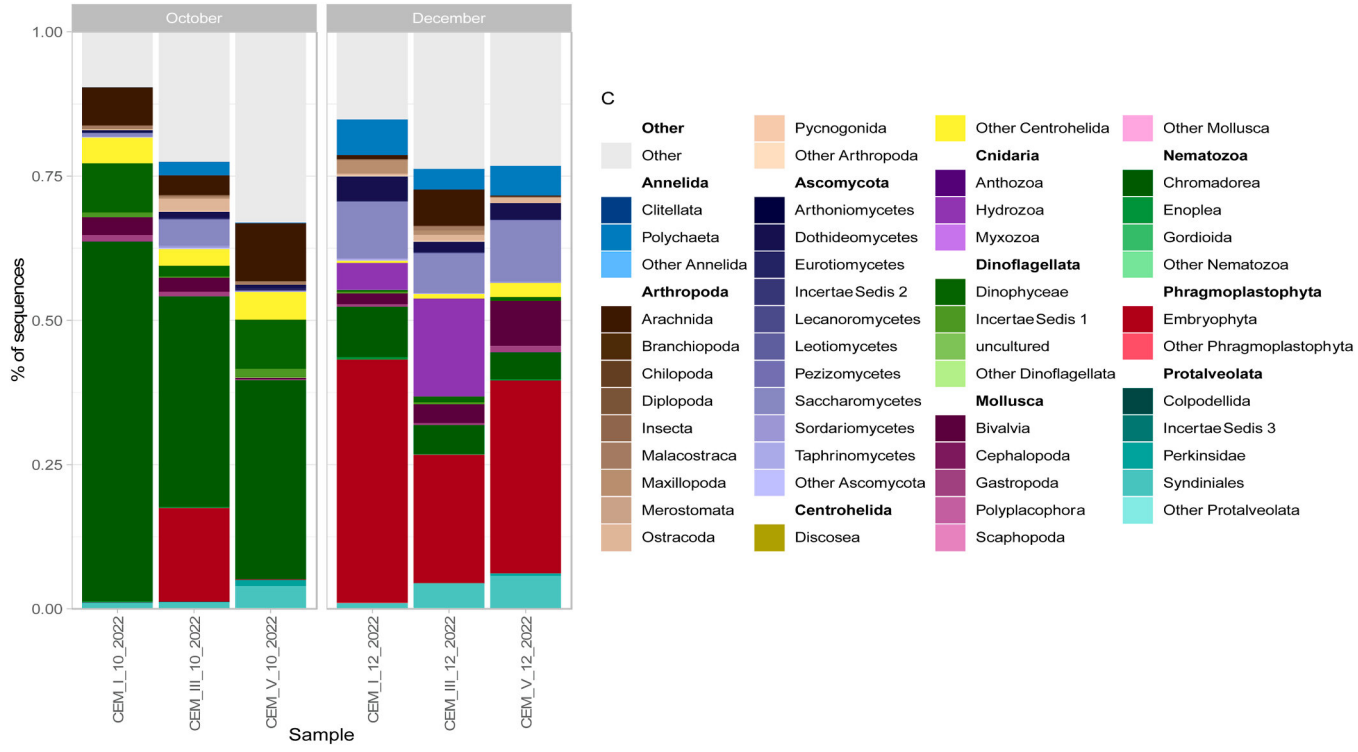


**Fig. 5.** From left to right: Eukaryotic diversity (18S rRNA genetic sequences) of marine biofilms colonizing the three different types of cement immersed for 30 (October) and 90 (December) days.

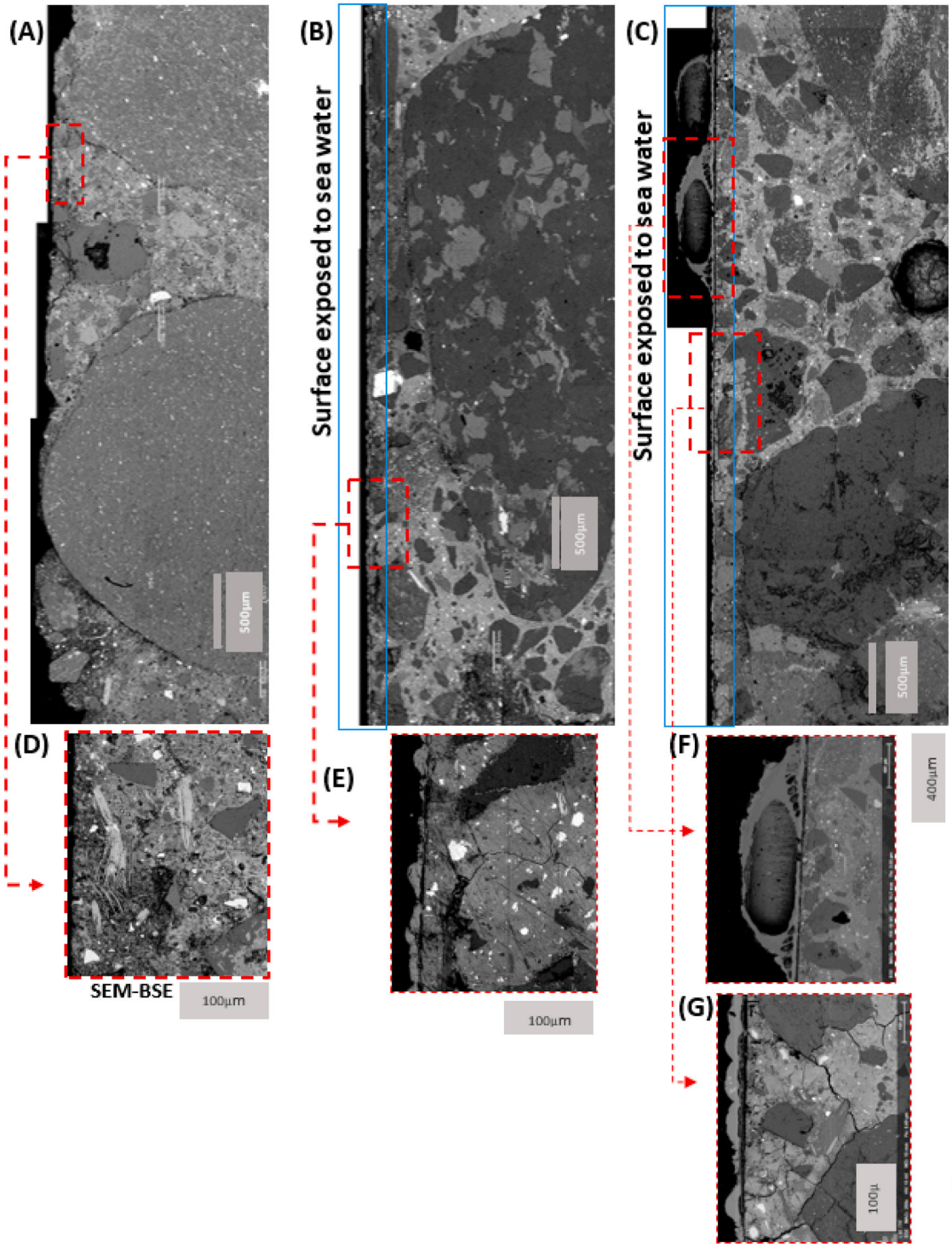


**Fig. 6.** SEM observations (BSE mode) of top surface of CEM I concrete; Overview of top surface of control (A), after 30 - (B), and 90 days (C) of exposure to sea water. Higher magnification of a specific area of the top surface of control (D), and after 30 days (E). Specimens exposed for 90 days show the growth of serpulid species on the concrete surface: cross-section of serpulid tube (F), and area without macrofouling species (G).

### *3.5. Characterization of altered and control concrete specimens*

The changes in microstructural, chemical oxide compositions, and mineralogy in control and concrete specimens exposed to seawater for 30 and 90 days are presented below.

#### *3.5.1. CEM I concrete*

*3.5.1.1. Microstructural and chemical characterization.* Fig. 6 depicts microstructural observations performed with a scanning electron microscope in back scattered electron mode of the top layer of CEM I control concrete (A) and exposed to seawater for 30 (B) and 90 days (C).

A clear distinction can be made between control and specimens exposed to seawater. As shown in Fig. 6A, in control concrete, the

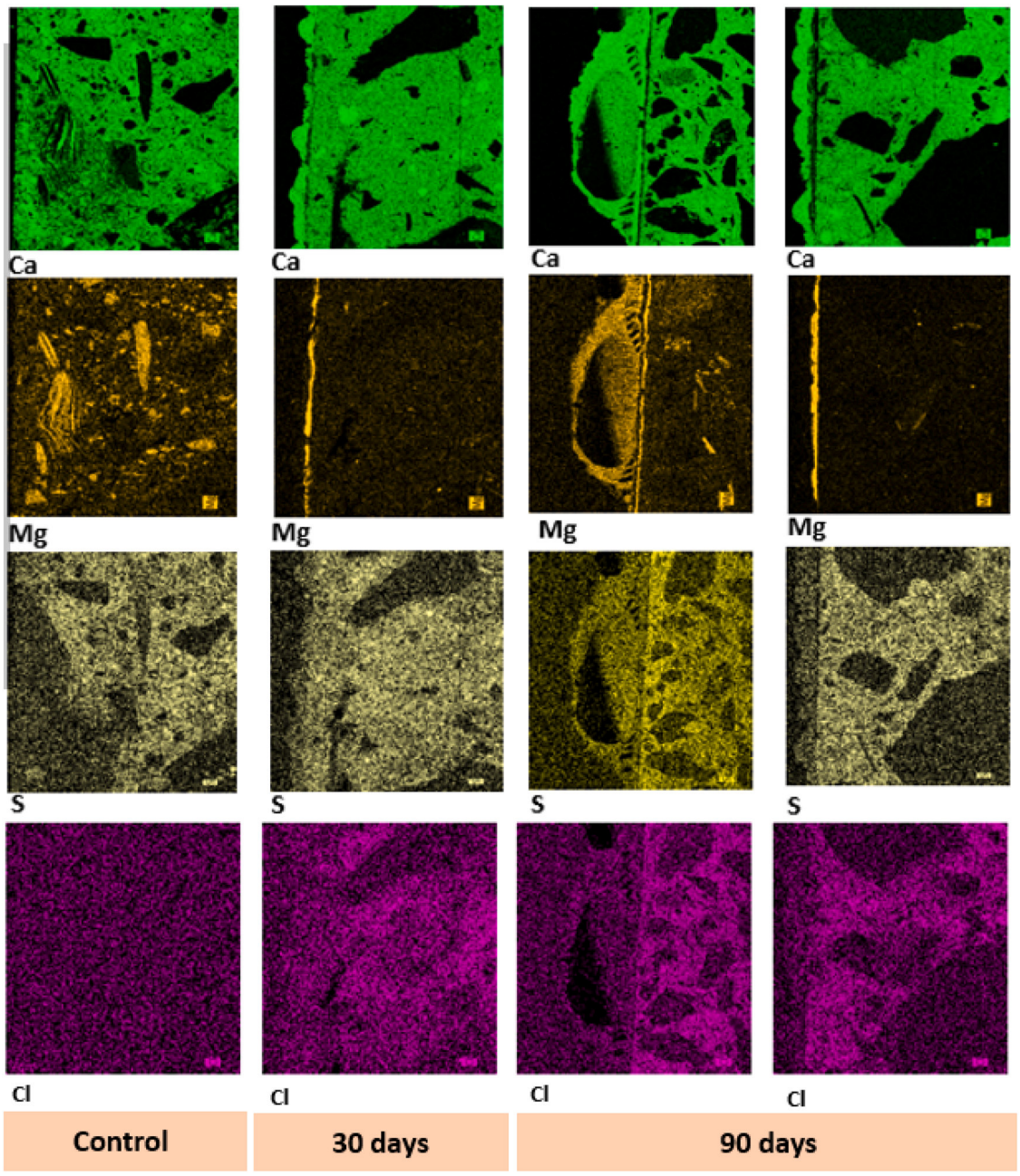


**Fig. 7.** Elemental mapping by SEM-EDS of BSE images in Fig. 10 (D), (E), (F), and (G) at 30 and 90 days of exposure to seawater.

topmost layer consists of big aggregates along with the distribution of smaller aggregates in between the cement paste. The brightest areas in terms of grey scale in the cement paste correspond to the denser phases, i.e., anhydrous cement grains, while black color indicates pores, and intermediate grey levels correspond to the hydrated cement matrix, composed mainly of calcium silicate aluminate hydrates (C-A-S-H), calcium hydroxide, and calcium aluminate hydrate phases, and aggregates. There is moderate contrast between aggregates and cement paste. While in the specimens exposed for 30 days (Fig. 6B and E), we noticed the development of a uniform, thin, and dense deposit on the top layer in contact with seawater and biofilm (visual inspections revealed a thin layer of slimy biofilm over this crust). Within this deposit, a distinct and uniform thin layer (less contrast in appearance underneath the deposit) is noticeable. The cracks visible on the specimen (Fig. 6E) are likely caused while sawing the sample for SEM-EDS analysis. Beneath this layer, cement paste has considerable density and compactness. The most striking feature observed for concrete specimens exposed to sea water for 90 days is the growth of biogenic and biomineral (inorganic minerals produced by organisms in natural seawater [52]) macrofouling species, serpulid tube worms on its outer layer (with overlying biofilm). The overview of the transverse cross-section of the surface deposit along with serpulid tubular wall is shown in Fig. 6C. The tubular shell was found to be several hundred microns in thickness, and concentric layers of slightly different contrast was observed. It is interesting to note that some areas on the outer layer of concrete surface were covered with these macrofouling organisms, while the remaining were uncovered. There is no discernable difference in contrasts between the serpulid tube wall and the precipitated scale deposit. This might be due to similarity in the chemical composition. Just beneath the serpulid tubular wall, a thin interfacial layer can be seen. SEM observations suggest that the characteristics of cement paste in the core are like those observed at 30 days of exposure.

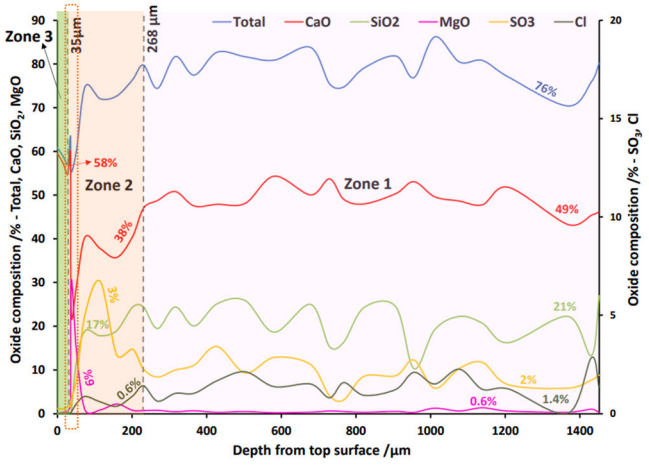


**Fig. 8.** Chemical composition profile of cement matrix in CEM I concrete after 90 days exposure to seawater with total, CaO, $SiO_2$, MgO, $SO_3$, and Cl analyzed by EPMA. The dotted red rectangle over MgO composition indicates an Mg-rich layer.

Fig. 7 shows the EDS elemental maps providing the elemental distribution of various elements in concrete. SEM coupled to EDS reveals the chemical concentration of individual elements such as calcium, magnesium, sulphur, and chlorine. The brightness of the elemental 2D images is determined by the relative concentration of the element. After 30 and 90 days, we observe significant calcium deposits on the outer layer of exposed specimens. A distinct layer of magnesium-rich zone (orange) lies beneath this deposit. As soon as this Mg-enriched zone ends, sulphur-rich (light yellow), and chlorine-rich (pink) zones appear. Comparing 30 and 90-day exposed specimens, we see that the Cl-rich zone begins shortly after the S-rich zone at 30 days, whereas the S-rich and Cl-rich zones overlap at 90 days.

*3.5.1.2. Chemical composition profiles characterized using EPMA.* The focus of electron microprobe analysis was specifically on chemical composition of hydrated cement paste, with the exclusion of aggregates and anhydrous cement grains. Figure S3 (in supplementary material) and Fig. 8 depict the chemical variations of various compounds across the specimen as a function of distance to the surface in contact with seawater and biofilm measured by EPMA after 30 and 90 days of exposure. The three zones are divided based on the variation of calcium pattern, (1) the internal/core zone, (2) a transition zone extending from the surface to a general depth of about 220 micrometers, and (3) the scale deposit. The chemical composition profiles obtained from EPMA are consistent with the elemental maps generated through SEM-EDS technique.

The analysis of the specimen exposed to seawater for 30 days (Figure S3, included in the supplementary material) indicates the following:

- Zone 1 or the internal zone, from 250 µm from the surface, maintains a uniform concentration of CaO, which corresponds to the CaO content of the control specimen. It is important to note that the local fluctuations in average $SiO_2$ content from the transition zone across the specimen remain relatively constant. Furthermore, the average magnesium oxide content in the internal zone has decreased relatively. Regarding chloride concentration in this zone, it reaches a maximum of 0.7 %, compared to 0.035 % in the control, indicating that chloride ions have diffused through the porosity and bound to the cement matrix.
- CaO content in Zone 2 or transition zone is 41 %, which translates to very mild decalcification. Further chemical analyses reveal a magnesium-rich layer beneath the scale deposit with an average content of 0.7 %, while this transition zone has the highest $SO_3$ content, 2.9 %. The $SO_3$ content increases at 120 µm and then remains steady. The concentration of chlorides increases from the surface inwards, following the chemical line from 200 µm.
- The crust is a calcium-rich surface deposit. It is the outer layer having 35 µm in thickness. The average CaO composition in this zone reaches 61 % by mass, with other contents such as $SiO_2$, MgO, $SO_3$, and Cl having negligible content in comparison to the following two zones.

The chemical oxide composition profile measured by EPMA for specimens exposed for 90 days is shown in Fig. 8. For this analysis, points were chosen on hydrated cement phases beneath the calcareous serpulid tube. As we move from internal zone to the deposit surface:

- The chemical pattern lines in the internal zone, or Zone 1, for CaO, MgO and sulphates, are similar to 30-day exposed specimens. However, the concentration of chlorides has reached 1.4 %. Additionally, sulphur-rich and chlorine-rich zones overlap as seen in elemental mapping (shown in Fig. 7).
- Zone 2, or transition zone extends between 35 µm and 268 µm. The concentration of CaO drops to 38 %, while MgO increases to 6 %. The chemical composition presented here supports the elemental maps that show a thick Mg layer. Thereafter, passage of $SO_3$ is the highest in the middle of transition zone, followed by uniform highs and lows across the specimen.
- The crust is a calcium-rich deposit with the same thickness as the 30-day exposed specimen and has a CaO concentration of 58 % on average It is noticeable from SEM image (Fig. 6) that this deposit has been covered with calcareous serpulid tubes. At various points within the calcareous serpulid tubular wall, we identified different locations and determined the calcium oxide (CaO) and magnesium oxide (MgO) compositions, calculating and averaging them accordingly. The chemical compositon of CaO is 50 ±0.9 %, and MgO is 7 ±0.6 %. These findings are consistent with elemental maps in Fig. 7.

*3.5.1.3. Characterization of mineral phases using X-ray diffraction.* Fig. 9A shows the XRD pattern of scale deposit (or calcium crust) and the surface at 15 mm of CEM I concrete characterized by XRD analysis after 30 and 90 days of exposure along with control specimen. Aggregates comprise most of the concrete composition, with quartz being the most common mineral. This made it more difficult to determine the peak diffraction patterns of most crystallized phases, including anhydrous and hydrated compounds. After 30 and 90 days, the scale deposit consists of calcium carbonate and calcite peaks, with aragonite polymorph peaks being predominant. Diffraction peaks of calcium hydroxide (CH), quartz, calcium aluminum silicate (CAS), anorthoclase, albite-calcian (peaks corresponding to aggregate minerals) were identified at 15 mm surface. To identify the magnesium-rich minerals, the top surface of the 30-day-exposed CEM I specimen was gently polished (with 1200 micron SiC discs). Fig. 9B depicts the diffractogram of peaks associated with brucite ($Mg(OH)_2$), aragonite, calcite, and quartz minerals.

*3.5.2. CEM III and CEM V*

*3.5.2.1. Microstructural, chemical composition, and mineralogical characterization.* The SEM-EDS observations and analyses for CEM III and CEM V concrete differ from those for CEM I in the following ways: (a) there was no significant calcium-rich deposition, (b) regardless of the exposure duration, no distinct Mg-rich layer was observed in the elemental maps, and (c) an interfacial layer beneath the serpulid tubular wall seems to be absent. It is interesting to note the uniform distribution of magnesium spots throughout the cement matrix in CEM III and CEM V cement types. After one month exposure, elemental maps of CEM V concrete show that presence of chloride ions is almost non-existent;

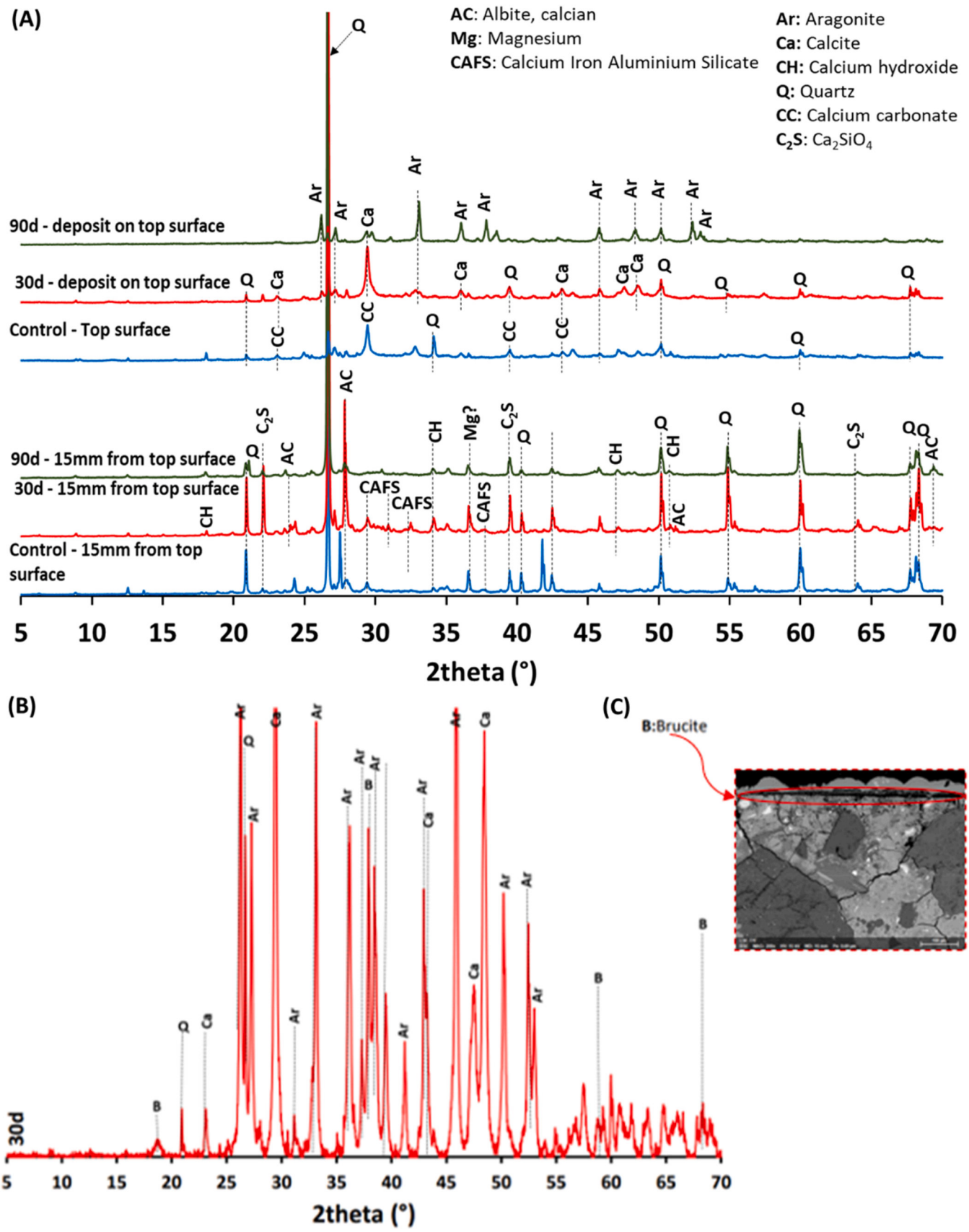


**Fig. 9.** (A) XRD patterns of scale deposit on top surface and its surface at 15 mm of CEM I concrete and control specimen (2theta-CuKα); (B) An XRD pattern obtained after gentle polishing of the $CaCO_3$ scale deposit, revealing brucite mineral in CEM I concrete after 30 days of exposure;(C) SEM image of top surface of CEM I concrete at 200x (100 μm) magnification indicating brucite layer.

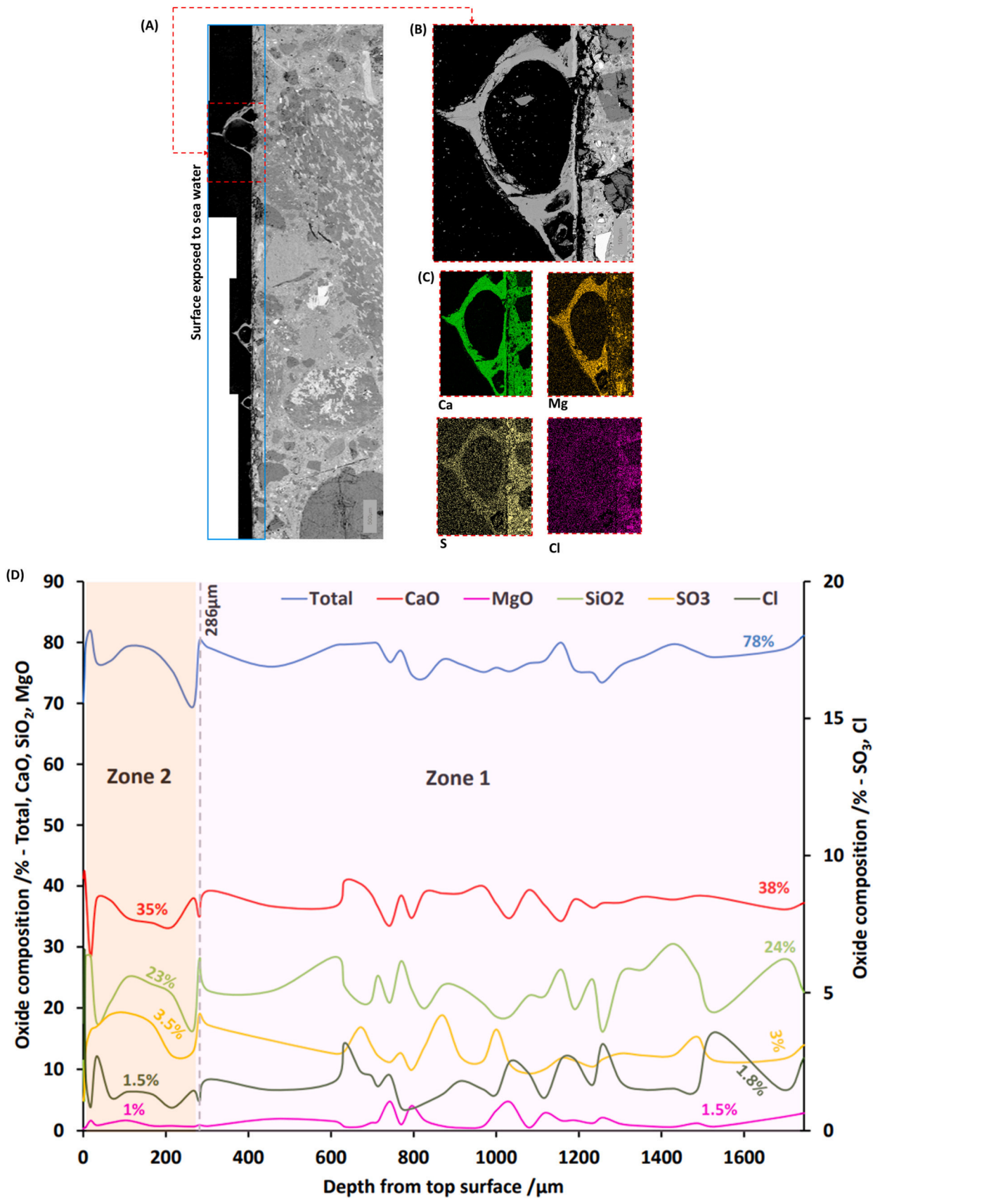


**Fig. 10.** (A) Overview of top surface of CEM V concrete after 90-day exposure to seawater; (B) Cross-section of serpulid tube in BSE mode; (C) Elemental maps of (B); (D) Chemical composition profile of cement matrix in CEM V concrete after 90 days exposure to seawater with total, CaO, $SiO_2$, MgO, $SO_3$, and Cl analyzed by EPMA.

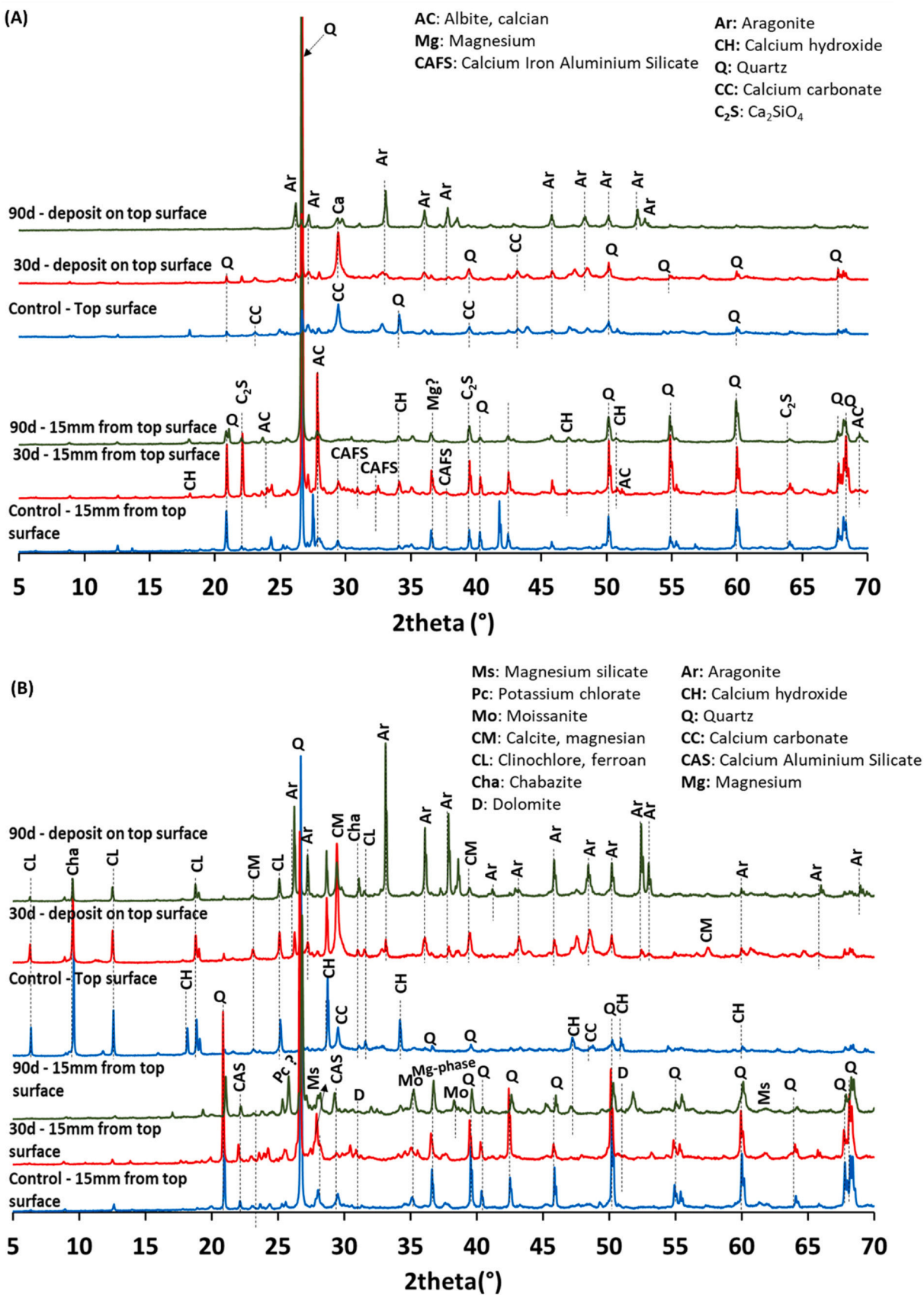


**Fig. 11.** From left to right: XRD patterns of concrete surface and the surface at 15 mm for (A) CEM III and (B) CEM V cement types for control, after 30- and 90- days exposure to natural seawater.

however, appears following three months exposure, with overlapping of S- and Cl- zones (Fig. 10C).

The average chemical oxide composition obtained by EPMA for CEM III and CEM V control concrete is shown in Table 4. The electron microprobe findings for CEM III and CEM V concrete are presented here (shown in Fig. 10D and Figure S7 in supplementary material), showing significant differences from CEM I concrete. Consistent with the SEM-EDS results, the division of chemical zonation is slightly different from CEM I concrete due to the absence of thick calcium deposit in CEM III and CEM V concrete after exposure to seawater. Therefore, based on the patterned variations in sulphate concentration in these two cements, we divide it into two zones, (1) the internal zone/core, and (2) transition zone.

In the case of CEM III concrete, the thickness of calcium scale deposit is limited to 3 μm (shown in Figure S7 of the supplementary material). Irrespective of exposure time, the overall percentage of calcium oxide is almost the same as control. In contrast to CEM I concrete, which exhibited high levels of magnesium oxide precipitation on the top surface, the distribution of magnesium oxide in CEM III concrete remains consistent throughout the specimen. Moving to $SO_3$ content, we notice a general trend of increase from the transition zone with a sharp peak as we enter the internal zone at both immersion times. In the interior zone (or Zone 1), overlapping of chloride and $SO_3$ chemical lines is conspicuous. The changes in $SO_3$ content after one month and three months are 7 % and 4.3 % respectively within the transition zone suggesting slight sulphur enrichment in the latter. For the internal zone, it goes up to 3.1 % and 3.5 % after one and three months respectively. Upon one month's exposure, there is less chlorine content (0.7 %) in the transition zone, but after three months, there is an increase to 2.5 %. From the end of the transition zone into the internal zone, the pattern and content of the chemical line for chlorine is nearly identical in both cases.

Fig. 10D shows the findings of EPMA for CEM V cement after three months exposure. The transition zone is 268 μm in length that lies before the internal zone. Despite elemental mapping revealing a calcium deposit on the outer layer, measurements from this analysis do not support this. Scarce amounts of calcium oxide are noticed at 18 μm, even though the overall CaO across the specimen (38 %) remains the same as in the control specimen. The patterned chemical variations in MgO content are same as the CEM III cement, alongside, the concentration is same as in control specimen. Sulphur content (3.5 %) is higher and closer to the outer layers, and as we approach the core, sulphur content (3 %) slightly increases between 700 and 1000 μm and then stabilizes. Sulphur and chlorine zones overlap from the outer layers, as indicated by elemental mapping, which is corroborated here. The percentage of chlorine content in the transition and internal zone is approximately the same (1.5 %).

We observed the development of serpulid tubes on both cement types at 90-day exposure. The chemical composition of the serpulid tubular walls was analyzed using the same approach employed for CEM I. For CEM III concrete, the composition was 51 %± 2.3 % of CaO and 6.2 %± 0.7 % of MgO, with CEM V concrete showing nearly identical results (CaO - 51 %± 2 % and MgO - 6 %±0.6 %).

*3.5.2.2. Characterization of mineral phases using X-ray diffraction.* Fig. 11A and B show the XRD patterns of the top surface with the calcium-bearing deposits and the internal surface at 15 mm of CEM III and CEM V concrete specimens respectively. CEM III and CEM V concrete, like CEM I concrete, exhibit several peaks associated with fine aggregates. This reduces the signal intensity corresponding to cement hydrate peaks, which can sometimes overlap, making them difficult to discern. The diffractogram of scale deposit at 90 days reveal aragonite crystal as the most dominant polymorph on CEM III and CEM V concrete surfaces. In the 15 mm surface of CEM III concrete, some of the cementitious phases present include calcium hydroxide and anhydrous phases such as calcium iron aluminum silicate and dicalcium silicate. Irrespective of time, the top surface of CEM V concrete indicates a few peaks corresponding to the presence of highly crystalline minerals like calcite magnesian(co-precipitation of $Mg^{2+}$ into $CaCO_3$ [53]), clinochlore ($(Mg)_5Al(AlSi_3O_{10})(OH)_8$ (aluminosilicate mineral [54]), and chabazite (zeolite ($CaAl_2Si_4O_{12}.6H_2O$) in OPC-fly ash blended cements [68]) peaks. At 15 mm from the top surface, calcium hydroxide, calcium aluminium silicate, dolomite, moissanite (mineral associated to fly ash content [55]) peaks are observed. The primary distinction in the mineral composition of exposed surfaces between CEM I and CEM V is the presence of a few peaks corresponding to calcite magnesian in the latter.

## 4. Discussion

The discussion below centers on the short-term interactions between biofouling, concrete, and seawater made from three cements in marine environments submerged at a depth of 27 m. It is organized into two sections, the first addressing the biodiversity on the concrete surface, while the second examining the alteration of concrete after exposure to natural seawater.

### *4.1. Biodiversity on the surface of concrete*

In this experimental program, we installed concrete specimens made of three types of cement to evaluate biofouling on the concrete surfaces after 30 and 90 days of exposure to seawater. As solid surfaces are typical hotspots for biofouling, assessment of microbial proliferation (or the biofilm development) at short-term is crucial to investigate long-term biofouling dynamics and predict potential changes in microbial communities of marine biofilms that could potentially influence the initiation of biodeterioration or bioprotection of concrete. Initial microbial colonization on concrete surface is influenced by the intrinsic properties of the material, including physical attributes like porosity, roughness, and hydrophobicity, and chemical properties such as chemical composition and surface pH [14,36]. Roughness, hydrophobicity, and surface pH has been a subject of work by *Hayek et al.* indicating that rough surfaces exhibit higher receptivity to initial microbial colonization [36]. In addition to the above-mentioned attributes, carbonated surfaces and slag-blended cement-based concrete demonstrate early receptivity to microbial colonization [14,36,56]. Furthermore, sustainable materials for the construction of floating offshore wind turbines, such as low-$CO_2$-binder systems, for example, slag-based blends should be prioritized, as done in this study. In light of this, a recent study conducted in the subtidal zone by *Bone et al.* [9] found that slag-based mortars had the lowest receptivity to biofouling compared to Portland cement and a natural Roman binder after one year of exposure. Their research has revealed that the differences in the biocolonization on surfaces, influenced by cement type, harbors, and ecological metrics, highlight the need for further investigation into the changes in the chemical composition of cement.

The primary biofilm community on the surfaces of cementitious materials like mortar and concrete in marine environments are like those found on other substrates, with bacteria and diatoms being the most predominant [57]. The FEG-SEM observations of the surface of mortars as shown in Fig. 3A, Fig. 3B, and Fig. 3C clearly indicate the presence of diatoms on mortars made of two cement types, namely, CEM III and CEM V at different exposure times. A recent study by *Georges et al.* demonstrated that the diatom species, *Cylindrotheca closterium* can assimilate dissolved silica from mortar surfaces in a silica-limited environment [58]. However, it remains unclear if the diatoms on the mortars in our study assimilate nutrients like silica from the cementitious matrix, given that natural seawater contains silica. The microbial communities identified through DNA-based-analysis were exclusively marine taxa, with *Alphaproteobacteria* and *Gammaproteobacteria* being the dominant groups in the biofilms, consistent with previous studies on artificial substrates in marine environments [59]. The comparison of bacterial

diversity on concrete surfaces made from CEM I, CEM III, and CEM V cement types revealed no significant statistical differences after 30 and 90 days of exposure. Notable bacterial species identified included *Bacillus*, *Sulphitobacter*, and *Pseudomonas*, known for altering natural substrates such as stone, were detected on the concrete surfaces as well [60]. Nevertheless, these species did not appear to influence the microstructure, chemical composition, and mineralogy of the concrete surfaces within this exposure duration.

*Qian et al.* have highlighted that the interaction between abiotic surfaces and the biofilms forming on these surfaces are influenced by differences in selective forces, which might explain the behavior observed on concrete surfaces [59]. Previous studies suggest that prokaryotic diversity in biofilms on various surfaces of substrates produce chemical cues that may influence microbial attachment as well as determine which type of microorganisms and larvae of macroorganisms settle [61–63]. While the diversity of prokaryotes in marine biofilms is well-documented, eukaryotic diversity has not received much attention. Meanwhile, our study has, for the first time, identified eukaryotic diversity on concrete surfaces made of three different types of cement (as shown in Fig. 5). Significant variations in the relative abundance of sequences in different eukaryotic groups were noted after 30 and 90 days of exposure to seawater. Although the eukaryotic diversity highlights arthropods, nematozoa, embryophytes, visual inspections, strikingly showed colonization by polychaetes (belonging to annelids class). These polychaetes are calcareous tube-building marine sessile organisms known to be common fouling species on a variety of substrates such as rocks, artificial substrates, coral reefs, in environments such as seawater, fresh water, and brackish water [64]. Yet, there is no information reported in the literature on the mechanism of how polychaetes grow and settle on concrete surfaces in seawater. There are several research studies that have been investigated in the past on the mechanism of growth of these species on substrate surfaces [65–68]. A study by *Nedved et al.* based on a laboratory experimental research proposed a model for biofouling using the serpulid tubeworm, *Hydroides elegans* [69]. They demonstrated that the larvae of these organisms are specifically induced from the biochemical cues of the biofilm consisting of bacterial communities. The larvae of these species attach themselves using adhesive secretions, mature in less than three weeks and metamorphosize into juvenile and adult forms. Due to their short larval phase, these tubeworms have the rapid ability to colonize substrates, including concrete surfaces [69]. Other marine invertebrates such as barnacles, tubeworms, and molluscs have the capacity to inhabit and establish colonies on hard substrates like corals, reefs, submerged artificial structures, limestone-based materials, and rocks as indicated in previous studies [70–72]. Interestingly, serpulid tubeworms were found to adhere firmly to concrete surfaces, demonstrating significant resistance to dislodgement. Additionally, a study conducted by *Hutchings et al.*, underscores the notion that polychaeta exhibit macroboring behavior in calcium carbonate-based corals [86]. But it is too early to say about the interactions between the polychaetes and concrete after 90-day exposure.

To our knowledge, this study is pioneering in examining the dynamic microbial communities on concrete surfaces made from three different cement types. This is characterized by combining a sequencing of 16S rRNA, 18S rRNA, and ITS markers at short-term, i.e., after 30 and 90 days of exposure to seawater at 27 m depth. However, the limitation of DNA barcoding is the difficulty in identifying many taxa due to lack of referencing of microbial sequences in public integrated databases. Future studies should emphasize the long-term monitoring and identification of microbial colonization and succession on concrete surfaces. Examining microbial diversity alongside the chemical characterization of concrete will strengthen our understanding of whether biodeterioration or bioprotection is favored. Additionally, it is vital to monitor changes in biofouling over time based on cement type to ascertain if the chemical composition of the cement supports specific species at submerged depths.

### 4.2. Deterioration of concrete in natural seawater

Natural seawater, with its complex mixture of organic and inorganic components and microorganisms, may affect the durability of concrete structures, depending on the marine exposure zone. In the submerged zone, concrete experiences less deterioration due to constant water saturation and limited oxygen, which may enhance hydration and result in a denser microstructure. However, it still remains vulnerable to multi-ion chemical attack and biofouling activity, which may deteriorate (or probably offer (bio) protection) concrete over time. This study compares the deterioration patterns of two low-$CO_2$-based cements, CEM III and CEM V, with conventional cement, CEM I, after 30- and 90-days exposure to natural seawater, focusing on multi-ion interactions involving calcium, magnesium, sulfur, and chloride. The findings highlight the changes in microstructure, chemical composition, and mineralogy as a function of cement type over time.

*Calcium scale deposit and serpulid formation:* After 30 and 90-day exposure periods, SEM-EDS investigations confirmed the presence of uniform calcium-rich scale deposit following the biofilm layer of concrete surfaces, irrespective of cement type. Additionally, electron microprobe analysis was used to quantify the mass percentage of calcium oxide as a function of depth. The results indicated that the deposit thickness on the concrete surface was significantly higher for CEM I ($\sim$ 35 μm) compared to CEM III and CEM V ($\sim$ 3 μm). The mineralogical characterization performed using XRD confirmed the presence of calcium carbonate and their polymorphs, namely, aragonite crystals on CEM I concrete surface at both exposure times, but not in CEM III or CEM V until 90 days. This is consistent with previous studies by *Buenfeld et al.* [73] and *Weerdt et al.* [11], [74] showing $CaCO_3$ deposit consisting of aragonite as the most dominant polymorph in Portland-based cements. The XRD pattern of the CEM V concrete surface revealed some peaks associated with magnesian calcite. Furthermore, the XRD pattern shows calcium carbonate peaks on control specimens of CEM I, III, and V concrete surfaces, which might be caused due to natural carbonation process [75]. The varying thickness of calcium carbonate precipitated layer as well as their mineralogy possibly indicate the influence of the cement type at both exposure periods. The hydrated calcium phases in the cement matrix differ considerably among the cement types studied. CEM I is characterized by a high calcium-to-silicon (Ca/Si) ratio, while CEM III and CEM V exhibit a lower Ca/Si ratio. The variations in Ca/Si ratios in cement matrix plausibly influence the reaction kinetics of calcium carbonate precipitation on the concrete surfaces in seawater. The carbonates participating in this precipitation reaction, deposited on the concrete surface may originate from pelagic sediments, which account for one-third of the total content in seawater [76]. This calcium carbonate mineral has three polymorphic modifications, namely, calcite, aragonite, and vaterite, with the former being the most thermodynamically stable in seawater and vaterite being least stable. The development of certain modifications in polymorphs via precipitation in aqueous solution is determined by the initial concentration of constituent ions, temperature, dissolved impurities, and, under certain conditions, suspended impurities [77,78]. Suspended silicate minerals are another commonly overlooked source, and if present in sufficient quantities, they contribute to the slight or moderate supersaturation of calcium carbonate polymorphs under these conditions [79]. Over time, specifically after 90 days, the precipitated calcium carbonate surfaces revealed the presence of biogenic and biomineral serpulid tubes. Visual observations and SEM images indicated the attachment of adult and juvenile polychaetes (serpulid tubes) on all the concrete surfaces. The local chemical composition of a cross-section of the serpulid tubular wall, analyzed using electron probe microanalysis (EPMA) and shown in Fig. 11, revealed that they were mainly composed of calcium oxide (CaO $\sim$ 51 %) and of magnesium oxide (MgO $\sim$ 6%). The mineral composition was confirmed using XRD (shown in Figs. 8, 9, and 10 in supplementary material). The XRD spectra for serpulid tubes present on CEM I concrete indicate peaks corresponding to two polymorphs of

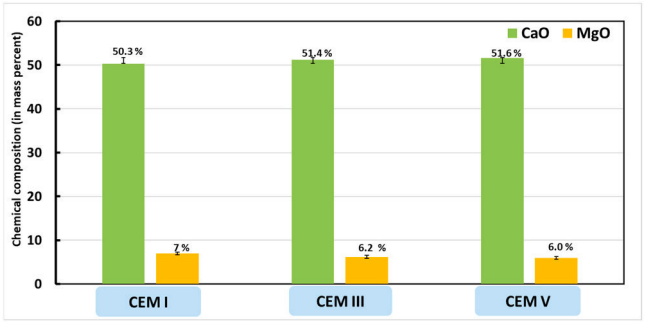


**Fig. 12.** Chemical composition of biogenic polychaetes on concrete surfaces of three cement types after 90 days exposure to seawater analyzed using electron microprobe analysis.

calcium carbonate: aragonite and Mg-calcite. The numerous peaks associated with aragonite crystals should be interpreted with caution. It is possible that calcium carbonate deposits on the CEM I concrete surface may have adhered to the serpulid tubes. When removing these species from the surface, these deposits may have been included in the analysis, potentially affecting the XRD analysis. In contrast, the diffractograms of serpulid tubes on surfaces of CEM III and CEM V concrete revealed only Mg-calcite (with traces of $SiO_2$ due to sand particles). It is interesting to note that these species are biomineral [94] in nature. Biomineralization is the process by which living organisms produce and control the precipitation of crystalline minerals. Our results are consistent with the literature indicating that the calcifying polychaetes are composed of different polymorphs of calcium carbonate [52,64]. Polychaetes develop in seawater through a series of biological processes, and their mineralogy and chemical composition are influenced by generic factors, water temperature, environmental conditions, and the Mg/Ca ratio in seawater [80,81]. Most biomineralized species such as sea urchins, mollusc shells, and corals consist of a single dominant polymorph of $CaCO_3$ [52]. Our results show Mg-calcite as the most dominant mineral of all three cement types. Moreover, the mineralogy of these serpulid tubes seem to be unaffected by the concrete surface and cement type within this exposure duration.

*Magnesium enriched zone:* Elemental mapping revealed a distinct layer rich in magnesium (Mg) beneath the calcium carbonate ($CaCO_3$) deposit at both 30 and 90 days in CEM I concrete (as shown in Fig. 7). In contrast, this layer was not observed in CEM III and CEM V cement types. This layer is composed of brucite crystals in CEM I concrete as shown in XRD analysis in Fig. 9. Magnesium, the second most abundant cation in natural seawater, may influence the kinetics of precipitation on concrete surfaces, varying with the type of cement used at submerged depths. Our findings suggest that the precipitation of brucite on concrete surfaces is likely dependent on the pH of the substrate. CEM III and CEM V, characterized as low-pH cements with pore solution pH between 11 and 12.5 (due to the presence of slag and fly ash), exhibit minimal or no portlandite in their hydrated matrices. The absence or minimal presence of portlandite in cement matrices creates different chemical conditions within the cement paste, which promote the precipitation of different magnesium hydrates. Several authors identify brucite precipitation at various exposure periods in CEM I cements, as well cements consisting of SCMs, which sometimes appear in cracks or within the $CaCO_3$ crust close to the top concrete surface exposed to marine environment [11,73]. However, it is important to note that in blended cements, brucite precipitation might occur at later stages of exposure in comparison to CEM I cement type [11]. Despite the ingress of seawater ions such as sulphates and chlorides into the cementitious matrix, magnesium ions do not travel deeper than other ions competing with them due to their small ionic radius and reactivity, as measured by electronegativity (1.31), and are more likely to deposit on the top surface [82,13]. According to the literature, this layer may function as a temporary barrier against other chemical ions, such as chlorides [83,12]. However, we raise doubts about this hypothesis. The substantial thickness of calcium carbonate deposits, along with the presence of biomineralized species on the concrete surface, might limit the ingress of chlorides and sulfates. This protective layer may be more effective than the brucite precipitated layer in enhancing concrete durability and reducing further deterioration.

In the aforementioned zone, elemental maps (as shown in Fig. 7) indicate slight leaching of $Ca(OH)_2$ in CEM I concrete after 30- and 90-days exposure. These findings are supported by EPMA, confirming that the decalcification front is deeper at 90 days, with ≅ 25 % of CaO

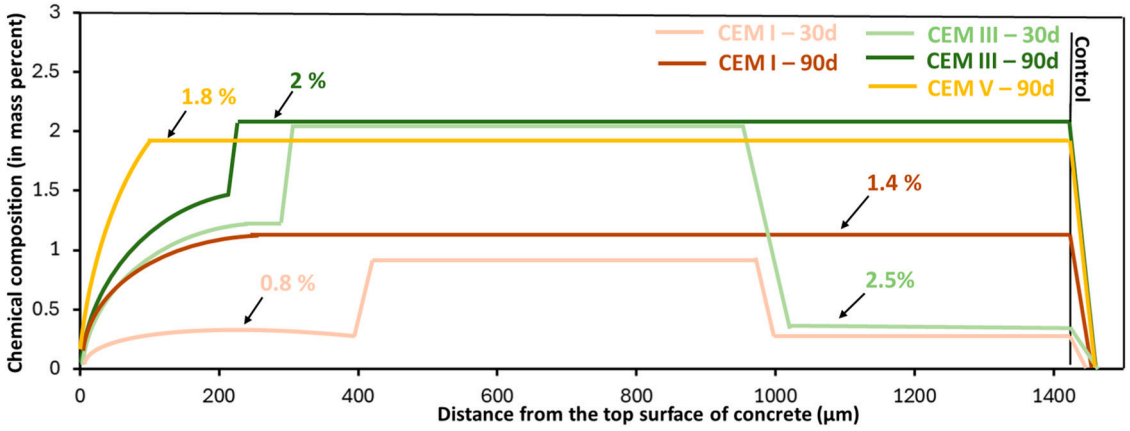


**Fig. 13.** Representative chloride profiles in three different cement matrices of concrete obtained through electron microprobe analysis at two exposure periods.

(control specimen having ~ 36 % of CaO). The data presented here are consistent with the literature, suggesting progressive phase dissolution-precipitation and diffusional stages [11]. The leaching of calcium from the cement matrix is a complex and multistage process observed primarily when the highly alkaline pore solution, saturated with portlandite (pKa = 12.6) within a sound cement matrix, interacts with a relatively acidic environment. In our study, this environment was represented by natural seawater, which typically has a pH between 7.5 and 8.5 [84]. This chemical equilibrium shift results in increased dissolution of calcium hydrates, notably portlandite, within the cement matrix. Consequently, dissolved calcium ions are leached into seawater and that might partly recombine to form calcium carbonate deposit on the surface, leading to a reduction in calcium content within the concrete. However, our SEM-EDS and electron microprobe investigations reveal no detectable calcium leaching from CEM III and CEM V concrete at both exposure times. This finding highlights the enhanced chemical resistance of these low-carbon-based cements to natural seawater at these exposure periods.

*Sulphur-enriched and chloride-enriched zone:* In a multi-ion environment such as natural seawater at submerged depths, chlorides and sulphates are in competition to penetrate and interact with the cement hydrates such as calcium hydroxide (CH), (unhydrated and hydrated) calcium aluminate hydrates ($C_xA_yH_z$), and calcium silicate aluminum hydrate (C-A-S-H) in the cement matrix. The combined attack of chlorides and sulphates depends on the content of calcium aluminate in cement matrix [85]. Our findings indicate that, when comparing control concrete (~3 %) to concrete exposed to seawater (between 3 % and 4.5 %) among different cement types, the chemical composition analyzed using an electron microprobe shows slight increase in sulfate concentration. The only exception is zone 2, which exhibits a slightly higher sulfate concentration ~3–4.5 %) than other zones (~3 %). Comparing concrete exposed for 30 and 90 days, CEM III and CEM V cement types exhibit increased sulfur concentration over time. However, the concentration of sulfate in CEM I remains nearly unchanged across both exposure durations. This stability may be attributed to the use of CEM I SR (sulphate resistant) cement in this study, which contains moderate alumina, reducing its capacity to react with sulfate. Irrespective of cement type and exposure period, microprobe analysis indicates that the concentration is slightly higher within the 100–300 μm depth range of the matrix. Despite CEM III and CEM V containing higher amounts of alumina, electron microprobe findings indicate that sulfur ingress and enrichment is almost the same in both cement types. This suggests that, within the exposure time of our study, alumina likely has no significant influence on sulfur reaction with cement matrix. Given the absence of cracks or spalling and no evident damage or attack during this short exposure, it is noteworthy that the observed changes may represent sulfur enrichment [11] rather than sulfate attack leading to gypsum and expansive ettringite formation at both exposure times. However, this might change with evolution of exposure time.

Chlorides, the most abundant anions in seawater, interact with hydrated cement compounds. Elemental maps and microprobe-analyzed profiles of concrete specimens reveal that Cl-rich zones often follow S-rich zones, with occasional overlaps between the two. The representative chloride profile for bound chlorides of three cement types at two exposure periods is depicted in Fig. 12. The chloride profile reveals varying binding capacities among the cement types, with CEM III and CEM V demonstrating greater binding than CEM I. Additionally, the saturation depth advances toward the internal zone over time. While the binder type appears to have little effect on the penetration depth, it significantly influences the chemical chloride binding. Irrespective of cement type, chloride ion penetration increases with the exposure duration. Our findings reveal that the surface of the concrete exhibits slightly lower chloride concentrations compared to the internal zones. Moreover, the chloride concentration decreases after 1100 μm, suggesting that, within the short-term exposure duration studied, chlorides have not penetrated deeply into the concrete. Previous research studies has shown that SCMs, such as GGBFS and fly ash, have a higher chloride-binding capacity due to higher alumina content in SCMs and a decrease in Ca/Si ratios in slag and fly ash, results in the formation of calcium aluminate silicate hydrate (C-A-S-H) and increase in chloride binding [86]. On the other hand, it is still unclear how the presence of the serpulid tubular walls along with the developed biofilm might alter the ingress of chloride ions into the cementitious matrix from the surface over time Fig. 13.

## 5. Conclusions

This study is the first to compare the durability of three cement types (CEM I, CEM III, and CEM V) in submerged marine environments, focusing on biofilm-concrete interactions using advanced and diverse analytical techniques. Conducted in real-world marine conditions, it provides more realistic insights than laboratory tests. Environmental DNA analysis revealed that bacterial colonization, irrespective of cement type or exposure time, serves as an essential metric in biofilm formation, while eukaryotic communities showed dynamic changes over time but not by cement type. The findings suggest that cement type does not influence biofilm structuring within the first 90 days of exposure. Short-term findings also indicate that CEM III and CEM V are more resistant to calcium leaching than CEM I, due to the presence of supplementary cementitious materials (SCMs) like slag and fly ash. Additionally, the deposition of calcium carbonate and biomineralized species on concrete surfaces may play a role in long-term durability. The absence of brucite precipitation in CEM III and CEM V, in contrast to its presence in CEM I, aligns with the literature but may alter over time. Furthermore, variations in chemical chloride-binding across concrete depths indicate that CEM III and CEM V have a greater chloride-binding potential than CEM I at these depths. These results can be effectively utilized in the design of sustainable and durable structures for harsh environmental conditions. Future research should focus on examining the long-term durability of different cement types at these depths, as well as identifying the microbial diversity in marine biofilms that may contribute to biodeterioration or bioprotection. This would provide insights into the associated changes in the microstructure, chemical composition, and mineralogy of concrete.

## CRediT authorship contribution statement

**Marie Salgues:** Writing – review & editing, Supervision, Project administration, Methodology, Investigation, Conceptualization. **Manon Thueux:** Methodology, Investigation. **Deeksha Margapuram:** Writing – original draft, Visualization, Methodology, Investigation, Formal analysis, Data curation, Conceptualization. **Fabrice Deby:** Supervision. **Carole Veckerlé:** Software, Methodology, Investigation, Formal analysis. **Florian Stratta:** Resources, Methodology. **Jean-Claude Souche:** Resources, Methodology. **Laurent Zudaire:** Resources, Methodology. **Bruno Hesse:** Resources, Investigation. **Renaud Vuillemin:** Resources, Methodology. **Michel Groc:** Resources, Methodology. **Alexandra Bertron:** Writing – review & editing, Supervision, Resources, Project administration, Methodology, Funding acquisition, Conceptualization. **Benjamin Erable:** Writing – review & editing, Supervision, Resources, Conceptualization. **Emilie Adouane:** Software, Formal analysis. **Raphaël Lami:** Writing – review & editing, Software, Investigation, Formal analysis, Conceptualization.

## Declaration of Competing Interest

The authors declare that they have no known competing financial interests or personal relationships that could have appeared to influence the work reported in this research paper.

## Acknowledgements

The authors are grateful to the Region Occitanie for its financial support (DuMaCoBio project), to the Wind'Occ agency for its federation and connection support during the construction and operation of the project, as well as Bio2Mar (K. Escoubeyrou) and Remimed technical platforms.

## Appendix A. Supporting information

Supplementary data associated with this article can be found in the online version at doi:10.1016/j.conbuildmat.2024.138840.

## Data availability

Data will be made available on request.

## References

[1] Shukla, R. Priyadarshi, Jim Skea, Raphael Slade, A. Al Khourdajie, R. Van Diemen, D. McCollum, M. Pathak, et al., Climate change, Mitigation of climate change, Contrib. Work. Group III sixth Assess. Rep. Intergov. Panel Clim. Change 10 (2022) (2022), 9781009157926.

[2] M. Maktabi, E. Rusu, A review of perspectives on developing floating wind farms, Inventions 9 (2) (Feb. 2024) 24, https://doi.org/10.3390/inventions9020024.

[3] M. Shafiee, Failure analysis of spar buoy floating offshore wind turbine systems, Innov. Infrastruct. Solut. 8 (1) (Jan. 2023) 28, https://doi.org/10.1007/s41062-022-00982-x.

[4] A. Mathern, C. Von Der Haar, S. Marx, Concrete support structures for offshore wind turbines: current status, challenges, and future trends, Energies 14 (7) (Apr. 2021) 1995, https://doi.org/10.3390/en14071995.

[5] E. Baita-Saavedra, et al., An economic analysis of an innovative floating offshore wind platform built with concrete: the SATH® Platform, Appl. Sci. 10 (11) (May 2020) 3678, https://doi.org/10.3390/app10113678.

[6] A. Witte, N. Garg, Quantifying the global warming potential of low carbon concrete mixes: comparison of existing life cycle analysis tools, Case Stud. Constr. Mater. 20 (Jul. 2024) e02832, https://doi.org/10.1016/j.cscm.2023.e02832.

[7] Y. Yi, D. Zhu, S. Guo, Z. Zhang, C. Shi, A review on the deterioration and approaches to enhance the durability of concrete in the marine environment, Cem. Concr. Compos. 113 (Oct. 2020) 103695, https://doi.org/10.1016/j.cemconcomp.2020.103695.

[8] M. Santhanam, M. Otieno, Deterioration of concrete in the marine environment. in Marine Concrete Structures, Elsevier, 2016, pp. 137–149, https://doi.org/10.1016/B978-0-08-100081-6.00005-2.

[9] J.R. Bone, A.E. Hall, R. Stafford, R.J.H. Herbert, Inconsistent bioreceptivity of three mortar mixes in subtidal sites, Ecol. Eng. 204 (Jul. 2024) 107265, https://doi.org/10.1016/j.ecoleng.2024.107265.

[10] M. Georges, A. Bourguiba, D. Chateigner, N. Sebaibi, M. Boutouil, The study of long-term durability and bio-colonization of concrete in marine environment, Environ. Sustain. Indic. 10 (Jun. 2021) 100120, https://doi.org/10.1016/j.indic.2021.100120.

[11] U.H. Jakobsen, K. De Weerdt, M.R. Geiker, Elemental zonation in marine concrete, Cem. Concr. Res. 85 (Jul. 2016) 12–27, https://doi.org/10.1016/j.cemconres.2016.02.006.

[12] K. De Weerdt, H. Justnes, M.R. Geiker, Changes in the phase assemblage of concrete exposed to sea water, Cem. Concr. Compos. 47 (Mar. 2014) 53–63, https://doi.org/10.1016/j.cemconcomp.2013.09.015.

[13] Chabrelie, A., Gallucci, E., Scrivener, K., & Müller, U. (2008, November). Durability of field concretes made of Portland and silica fume cements under sea water exposure for 25 years. In Nordic Exposure Sites—Input to Revision of EN206-1, Workshop Proceeding from a Nordic Miniseminar, Hirtshals—Denmark.

[14] J.R. Bone, R. Stafford, A.E. Hall, R.J.H. Herbert, The intrinsic primary bioreceptivity of concrete in the coastal environment – A review, Dev. Built Environ. 10 (May 2022) 100078, https://doi.org/10.1016/j.dibe.2022.100078.

[15] S. Ido, P.-F. Shimrit, Blue is the new green – Ecological enhancement of concrete based coastal and marine infrastructure, Ecol. Eng. 84 (Nov. 2015) 260–272, https://doi.org/10.1016/j.ecoleng.2015.09.016.

[16] K.L. Davis, M.A. Coleman, S.D. Connell, B.D. Russell, B.M. Gillanders, B.P. Kelaher, Ecological performance of construction materials subject to ocean climate change, Mar. Environ. Res. 131 (Oct. 2017) 177–182, https://doi.org/10.1016/j.marenvres.2017.09.011.

[17] M. Georges, A. Bourguiba, D. Chateigner, N. Sebaibi, M. Boutouil, The study of long-term durability and bio-colonization of concrete in marine environment, Environ. Sustain. Indic. 10 (Jun. 2021) 100120, https://doi.org/10.1016/j.indic.2021.100120.

[18] S. Karačić, O. Modin, P. Hagelia, F. Persson, B.-M. Wilén, The effect of time and surface type on the composition of biofilm communities on concrete exposed to seawater, Int. Biodeterior. Biodegrad. 173 (Sep. 2022) 105458, https://doi.org/10.1016/j.ibiod.2022.105458.

[19] T. Chlayon, M. Iwanami, N. Chijiwa, Combined protective action of barnacles and biofilm on concrete surface in intertidal areas, Constr. Build. Mater. 179 (Aug. 2018) 477–487, https://doi.org/10.1016/j.conbuildmat.2018.05.223.

[20] H.-C. Flemming, Why Microorganisms Live in Biofilms and the Problem of Biofouling, in Marine and Industrial Biofouling, vol. 4, in: H.-C. Flemming, P. S. Murthy, R. Venkatesan, K. Cooksey (Eds.), in Springer Series on Biofilms, 4, Springer Berlin Heidelberg, Berlin, Heidelberg, 2009, pp. 3–12, https://doi.org/10.1007/978-3-540-69796-1_1. in *Marine and Industrial Biofouling*, vol. 4.

[21] C.C. Gaylarde, B.O. Ortega-Morales, Biodeterioration and chemical corrosion of concrete in the marine environment: too complex for prediction, Microorganisms 11 (10) (Sep. 2023) 2438, https://doi.org/10.3390/microorganisms11102438.

[22] J.R. Bone, R. Stafford, A.E. Hall, R.J.H. Herbert, Biodeterioration and bioprotection of concrete assets in the coastal environment, Int. Biodeterior. Biodegrad. 175 (Nov. 2022) 105507, https://doi.org/10.1016/j.ibiod.2022.105507.

[23] P. Hughes, et al., Microscopic study into biodeterioration of marine concrete, Int. Biodeterior. Biodegrad. 79 (Apr. 2013) 14–19, https://doi.org/10.1016/j.ibiod.2013.01.007.

[24] Z. Liu, L. Gan, H. Rong, Durability of concrete exposed to laboratory-simulated marine microbe-induced corrosion, Constr. Build. Mater. 400 (Oct. 2023) 132563, https://doi.org/10.1016/j.conbuildmat.2023.132563.

[25] M.A. Coombes, E.C. La Marca, L.A. Naylor, R.C. Thompson, Getting into the groove: opportunities to enhance the ecological value of hard coastal infrastructure using fine-scale surface textures, Ecol. Eng. 77 (Apr. 2015) 314–323, https://doi.org/10.1016/j.ecoleng.2015.01.032.

[26] S. Jayakumar, R. Saravanane, Biodeterioration of coastal concrete structures by Macro algae - Chaetomorpha antennina, Mater. Res. 12 (4) (2009) 465–472, https://doi.org/10.1590/S1516-14392009000400015.

[27] P. Vuong, A. McKinley, P. Kaur, Understanding biofouling and contaminant accretion on submerged marine structures, Npj Mater. Degrad. 7 (1) (Jun. 2023) 50, https://doi.org/10.1038/s41529-023-00370-5.

[28] M. Salta, J.A. Wharton, Y. Blache, K.R. Stokes, J. Briand, Marine biofilms on artificial surfaces: structure and dynamics, Environ. Microbiol. 15 (11) (Nov. 2013) 2879–2893, https://doi.org/10.1111/1462-2920.12186.

[29] K. Rajitha, Y.V. Nancharaiah, V.P. Venugopalan, Insight into bacterial biofilm-barnacle larvae interactions for environmentally benign antifouling strategies, Int. Biodeterior. Biodegrad. 149 (Apr. 2020) 104937, https://doi.org/10.1016/j.ibiod.2020.104937.

[30] Y. Kawabata, E. Kato, M. Iwanami, Enhanced long-term resistance of concrete with marine sessile organisms to chloride ion penetration, J. Adv. Concr. Technol. 10 (4) (Apr. 2012) 151–159, https://doi.org/10.3151/jact.10.151.

[31] T. Chlayon, M. Iwanami, N. Chijiwa, Impacts from concrete microstructure and surface on the settlement of sessile organisms affecting chloride attack, Constr. Build. Mater. 239 (Apr. 2020) 117863, https://doi.org/10.1016/j.conbuildmat.2019.117863.

[32] M. Iwanami, H. Yokota, H. Hamada, T. Yamaji, H. Watanabe, Can Marine Fouling Organisms Extend the Life of Concrete Structures?. in IABSE Symposium, Melbourne 2002: Towards a Better Built Environment - Innovation, Sustainability, Information Technology International Association for Bridge and Structural Engineering (IABSE), Melbourne, Australia, 2002, pp. 84–91, https://doi.org/10.2749/222137802796337062.

[33] J. Lv, M. Wang, X. Hu, Z. Cao, H. Ba, Experimental study on the durability and microstructure of marine concrete covered with barnacles, Constr. Build. Mater. 317 (Jan. 2022) 125900, https://doi.org/10.1016/j.conbuildmat.2021.125900.

[34] AFNOR, 2016. NF EN 196–1. Methods of Testing Cement - Part 1: Determination of Strength (Paris, France).

[35] C.A. Schneider, W.S. Rasband, K.W. Eliceiri, NIH Image to ImageJ: 25 years of image analysis, Nat. Methods 9 (7) (Jul. 2012) 671–675, https://doi.org/10.1038/nmeth.2089.

[36] M. Hayek, M. Salgues, J.-C. Souche, E. Cunge, C. Giraudel, O. Paireau, Influence of the intrinsic characteristics of cementitious materials on biofouling in the marine environment, Sustainability 13 (5) (Mar. 2021) 2625, https://doi.org/10.3390/su13052625.

[37] C. Perez, C. Lors, B. Erable, Methodological approaches for the structural, chemical, and microbial analysis of microbial biofilms developed on the surface of cementitious materials: overview and future prospects, Int. Biodeterior. Biodegrad. 175 (Nov. 2022) 105485, https://doi.org/10.1016/j.ibiod.2022.105485.

[38] M. Romani, et al., High bacterial diversity in pioneer biofilms colonizing ceramic roof tiles, Int. Biodeterior. Biodegrad. 144 (Oct. 2019) 104745, https://doi.org/10.1016/j.ibiod.2019.104745.

[39] M. Romani, et al., Diversity and activities of pioneer bacteria, algae, and fungi colonizing ceramic roof tiles during the first year of outdoor exposure, Int. Biodeterior. Biodegrad. 162 (Aug. 2021) 105230, https://doi.org/10.1016/j.ibiod.2021.105230.

[40] B. Beckers, et al., Performance of 16s rDNA Primer Pairs in the Study of Rhizosphere and Endosphere Bacterial Microbiomes in Metabarcoding Studies, Front. Microbiol. 7 (May 2016), https://doi.org/10.3389/fmicb.2016.00650.

[41] F. Thomas, et al., Evaluation of a new primer combination to minimize plastid contamination in 16S rDNA metabarcoding analyses of alga-associated bacterial communities, Environ. Microbiol. Rep. 12 (1) (Feb. 2020) 30–37, https://doi.org/10.1111/1758-2229.12806.

[42] L.W. Hugerth, et al., Systematic Design of 18S rRNA Gene Primers for Determining Eukaryotic Diversity in Microbial Consortia, PLoS ONE 9 (4) (Apr. 2014) e95567, https://doi.org/10.1371/journal.pone.0095567.

[43] T. Cheng, C. Xu, L. Lei, C. Li, Y. Zhang, S. Zhou, Barcoding the kingdom Plantae: new PCR primers for *ITS* regions of plants with improved universality and

specificity,", Mol. Ecol. Resour. 16 (1) (Jan. 2016) 138–149, https://doi.org/10.1111/1755-0998.12438.
[44] W. Shen, S. Le, Y. Li, F. Hu, SeqKit: a cross-platform and ultrafast toolkit for FASTA/Q file manipulation, PLOS ONE 11 (10) (Oct. 2016) e0163962, https://doi.org/10.1371/journal.pone.0163962.
[45] D.E. Wood, J. Lu, B. Langmead, Improved metagenomic analysis with Kraken 2, Genome Biol. 20 (1) (Nov. 2019) 257, https://doi.org/10.1186/s13059-019-1891-0.
[46] C. Quast, et al., The SILVA ribosomal RNA gene database project: improved data processing and web-based tools, Nucleic Acids Res 41 (D1) (Nov. 2012) D590–D596, https://doi.org/10.1093/nar/gks1219.
[47] T.Z. DeSantis, et al., Greengenes, a Chimera-Checked 16S rRNA Gene Database and Workbench Compatible with ARB, Appl. Environ. Microbiol. 72 (7) (Jul. 2006) 5069–5072, https://doi.org/10.1128/AEM.03006-05.
[48] P.J. McMurdie, S. Holmes, phyloseq: an R package for reproducible interactive analysis and graphics of microbiome census data, PLoS ONE 8 (4) (Apr. 2013) e61217, https://doi.org/10.1371/journal.pone.0061217.
[49] A. Bertron, G. Escadeillas, P. De Parseval, J. Duchesne, Processing of electron microprobe data from the analysis of altered cementitious materials, Cem. Concr. Res. 39 (10) (Oct. 2009) 929–935, https://doi.org/10.1016/j.cemconres.2009.06.011.
[50] A. Bertron, G. Escadeillas, J. Duchesne, Cement pastes alteration by liquid manure organic acids: chemical and mineralogical characterization, Cem. Concr. Res. 34 (10) (Oct. 2004) 1823–1835, https://doi.org/10.1016/j.cemconres.2004.01.002.
[51] A. Bertron, J. Duchesne, G. Escadeillas, Accelerated tests of hardened cement pastes alteration by organic acids: analysis of the pH effect, Cem. Concr. Res. 35 (1) (Jan. 2005) 155–166, https://doi.org/10.1016/j.cemconres.2004.09.009.
[52] A.E. Tanur, N. Gunari, R.M.A. Sullan, C.J. Kavanagh, G.C. Walker, Insights into the composition, morphology, and formation of the calcareous shell of the serpulid Hydroides dianthus, J. Struct. Biol. 169 (2) (Feb. 2010) 145–160, https://doi.org/10.1016/j.jsb.2009.09.008.
[53] L. Mo, F. Zhang, M. Deng, Effects of carbonation treatment on the properties of hydrated fly ash-MgO-Portland cement blends, Constr. Build. Mater. 96 (Oct. 2015) 147–154, https://doi.org/10.1016/j.conbuildmat.2015.07.193.
[54] E.C. Gaucher, P. Blanc, Cement/clay interactions – A review: experiments, natural analogues, and modeling, Waste Manag 26 (7) (Jan. 2006) 776–788, https://doi.org/10.1016/j.wasman.2006.01.027.
[55] I. Kourti, C.R. Cheeseman, Properties and microstructure of lightweight aggregate produced from lignite coal fly ash and recycled glass, Resour. Conserv. Recycl. 54 (11) (Sep. 2010) 769–775, https://doi.org/10.1016/j.resconrec.2009.12.006.
[56] B.P. Guilbeau, F.P. Harry, R.P. Gambrell, F.C. Knopf, K.M. Dooley, Algae attachment on carbonated cements in fresh and brackish waters—preliminary results, Ecol. Eng. 20 (4) (Sep. 2003) 309–319, https://doi.org/10.1016/S0925-8574(03)00026-0.
[57] A. Car, D. Hafner, S. Ljubimir, I. Dupčić Radić, S. Bobanović-Ćolić, N. Jasprica, Colonization of bacteria and diatoms on an artificial substrate in a marine lake (eastern Adriatic Sea, NE Mediterranean), Acta Bot. Croat. 79 (2) (Oct. 2020) 212–227, https://doi.org/10.37427/botcro-2020-028.
[58] M. Georges, A. Bourguiba, M. Boutouil, D. Chateigner, O. Jolly, P. Claquin, Interaction between the diatom Cylindrotheca closterium and a siliceous mortar in a silica-limited environment, Constr. Build. Mater. 321 (Feb. 2022) 126277, https://doi.org/10.1016/j.conbuildmat.2021.126277.
[59] P.-Y. Qian, A. Cheng, R. Wang, R. Zhang, Marine biofilms: diversity, interactions and biofouling, Nat. Rev. Microbiol. 20 (11) (Nov. 2022) 671–684, https://doi.org/10.1038/s41579-022-00744-7.
[60] X. Li, et al., Analysis of cultivable aerobic bacterial community composition and screening for facultative sulfate-reducing bacteria in marine corrosive steel, J. Oceanol. Limnol. 37 (2) (Mar. 2019) 600–614, https://doi.org/10.1007/s00343-019-7400-1.
[61] P.D. Steinberg, S. Kjelleberg, Chemical Cues for Surface Colonization, J. Chem. Ecol. (2002).
[62] J.D. Zardus, B.T. Nedved, Y. Huang, C. Tran, M.G. Hadfield, Microbial biofilms facilitate adhesion in biofouling invertebrates, Biol. Bull. 214 (1) (Feb. 2008) 91–98, https://doi.org/10.2307/25066663.
[63] H.-U. Dahms, S. Dobretsov, P.-Y. Qian, The effect of bacterial and diatom biofilms on the settlement of the bryozoan Bugula neritina, J. Exp. Mar. Biol. Ecol. 313 (1) (Dec. 2004) 191–209, https://doi.org/10.1016/j.jembe.2004.08.005.
[64] O. Vinn, Biomineralization in polychaete annelids: a review, Minerals 11 (10) (Oct. 2021) 1151, https://doi.org/10.3390/min11101151.
[65] M.A.R. Koehl, M.G. Hadfield, Soluble settlement cue in slowly moving water within coral reefs induces larval adhesion to surfaces, J. Mar. Syst. 49 (1–4) (Aug. 2004) 75–88, https://doi.org/10.1016/j.jmarsys.2003.06.003.
[66] C.R.C. Unabia, M.G. Hadfield, Role of bacteria in larval settlement and metamorphosis of the polychaete Hydroides elegans, Mar. Biol. 133 (1) (Jan. 1999) 55–64, https://doi.org/10.1007/s002270050442.
[67] L.J. Walters, M.G. Hadfield, K.A. Del Carmen, The importance of larval choice and hydrodynamics in creating aggregations of hydroides elegans (Polychaeta: Serpulidae), Invertebr. Biol. 116 (2) (1997) 102, https://doi.org/10.2307/3226974.
[68] M.C. Gambi, G. Cafiero, Functional Diversity in the Posidonia oceanica Ecosystem: an Example with Polychaete Borers of the Scales, in: F.M. Faranda, L. Guglielmo, G. Spezie (Eds.), in Mediterranean Ecosystems, Springer Milan, Milano, 2001, pp. 399–405, https://doi.org/10.1007/978-88-470-2105-1_52.
[69] B.T. Nedved, M.G. Hadfield, Hydroides elegans (Annelida: Polychaeta): A Model for Biofouling Research, in Marine and Industrial Biofouling, vol. 4, in: H.-C. Flemming, P.S. Murthy, R. Venkatesan, K. Cooksey (Eds.), in Springer Series on Biofilms, 4, Springer Berlin Heidelberg, Berlin, Heidelberg, 2009, pp. 203–217, https://doi.org/10.1007/978-3-540-69796-1_11. in Marine and Industrial Biofouling, vol. 4.
[70] N. Pari, M. Peyrot-Clausade, P.A. Hutchings, Bioerosion of experimental substrates on high islands and atoll lagoons (French Polynesia) during 5 years of exposure, J. Exp. Mar. Biol. Ecol. 276 (1–2) (Sep. 2002) 109–127, https://doi.org/10.1016/S0022-0981(02)00243-5.
[71] E. Casoli, S. Ricci, F. Antonelli, C. Sacco Perasso, G. Ardizzone, M.F. Gravina, Colonization dynamic on experimental limestone substrata: the role of encrusting epilithics favouring boring polychaetes, Hydrobiologia 842 (1) (Oct. 2019) 101–112, https://doi.org/10.1007/s10750-019-04028-9.
[72] S. Marzialetti, L. Nicoletti, G.D. Ardizzone, The polychaete community of the Fregene artificial reef (Tyrrhenian Sea, Italy): a 20-year study (1981–2001), Zoosymposia 2 (2009) 551–566.
[73] N.R. Buenfeld, J.B. Newman, The development and stability of surface layers on concrete exposed to sea-water, Cem. Concr. Res. 16 (5) (Sep. 1986) 721–732, https://doi.org/10.1016/0008-8846(86)90046-3.
[74] K. De Weerdt, H. Justnes, The effect of sea water on the phase assemblage of hydrated cement paste, Cem. Concr. Compos. 55 (Jan. 2015) 215–222, https://doi.org/10.1016/j.cemconcomp.2014.09.006.
[75] A. Morandeau, M. Thiéry, P. Dangla, Investigation of the carbonation mechanism of CH and C-S-H in terms of kinetics, microstructure changes and moisture properties, Cem. Concr. Res. 56 (Feb. 2014) 153–170, https://doi.org/10.1016/j.cemconres.2013.11.015.
[76] J.W. Morse, F.T. Mackenzie, Geochemistry of sedimentary carbonates. Developments in sedimentology, Elsevier, Amsterdam, 1990.
[77] R. Brooks, L.M. Clark, E.F. Thurston, Calcium carbonate and its hydrates, Philos. Trans. R. Soc. Lond. Ser. A, Math. Phys. Sci. 243 (861) (1950) 145–167.
[78] Yasushi Kitano, Donald W. Hood, The influence of organic material on the polymorphic crystallization of calcium carbonate, Geochim. Et. Cosmochim. Acta 29 (1) (1965) 29–41.
[79] D. Kralj, N. Vdović, The influence of some naturally occurring minerals on the precipitation of calcium carbonate polymorphs, Water Res 34 (1) (Jan. 2000) 179–184, https://doi.org/10.1016/S0043-1354(99)00110-4.
[80] B.D. Bornhold, J.D. Milliman, Generic and Environmental Control of Carbonate Mineralogy in Serpulid (Polychaete) Tubes, J. Geol. 81 (3) (May 1973) 363–373, https://doi.org/10.1086/627876.
[81] X. Long, Y. Ma, L. Qi, Biogenic and synthetic high magnesium calcite – A review, J. Struct. Biol. 185 (1) (Jan. 2014) 1–14, https://doi.org/10.1016/j.jsb.2013.11.004.
[82] D. Bonen, M.D. Cohen, Magnesium sulfate attack on portland cement paste — II. Chemical and mineralogical analyses, Cem. Concr. Res. 22 (4) (Jul. 1992) 707–718, https://doi.org/10.1016/0008-8846(92)90023-O.
[83] W. Kurdowski, The protective layer and decalcification of C-S-H in the mechanism of chloride corrosion of cement paste, Cem. Concr. Res. 34 (9) (Sep. 2004) 1555–1559, https://doi.org/10.1016/j.cemconres.2004.03.023.
[84] S. Kamali, B. Gérard, M. Moranville, Modelling the leaching kinetics of cement-based materials—influence of materials and environment, Cem. Concr. Compos. 25 (4–5) (May 2003) 451–458, https://doi.org/10.1016/S0958-9465(02)00085-9.
[85] Maes M., Caspeele R., Van den Heede P., De Belie N. Influence of sulphates on chloride diffusion and the effect of this on service life prediction of concrete in a submerged marine environment. In: Strauss A., Frangopol D.M., Bergmeister K., editors. 3rd International symposium on Life-cycle Civil Engineering: Lifecycle and sustainability of civil infrastructure systems. Vienna, Austria; 2012.
[86] M.D.A. Thomas, R.D. Hooton, A. Scott, H. Zibara, The effect of supplementary cementitious materials on chloride binding in hardened cement paste, Cem. Concr. Res. 42 (1) (Jan. 2012) 1–7, https://doi.org/10.1016/j.cemconres.2011.01.001.